

# Fishing Bans in Chinese Waters: Effectiveness and Spillovers

Haishan Yuan\*

University of Queensland

November 4, 2024

## Abstract

China's large-scale seasonal fishing bans aim to promote sustainable fisheries, yet their effectiveness remains uncertain given the challenges of monitoring vast ocean areas. Using a novel dataset of nighttime vessel detections and a regression discontinuity in time (RDiT) design, we find that the bans reduce boat detections within China's Exclusive Economic Zone (EEZ) by 72%, with a sharp increase upon lifting. Boat detections also decline in neighboring EEZs at the start of China's bans, indicating regulatory spillovers. Data from AIS-equipped vessels reveal that Chinese boats operate in neighboring EEZs, while foreign vessels fish in the Chinese EEZ. Compliance weakens in the later stages of the bans, with more boats detected in areas with favorable conditions. Our findings suggest that command-and-control approaches can be effective for fishery management in contexts where market-based alternatives may not be practical. My findings also underscore the importance of addressing regulatory spillovers and strengthening complementary enforcement.

**Keywords:** Tragedy of the Commons; Regression Discontinuity in Time or Space; Fishing Ban; Fishery; Exclusive Economic Zone (EEZ); EEZ Incursion; Regulatory Spillover.

**JEL Classification Numbers:** Q22, Q56, Q58, K42, O13

---

\* Address: Level 6, Colin Clark Building (39), University of Queensland, St Lucia, QLD 4072, Australia; Email: h.yuan@uq.edu.au; I thank the editor, two anonymous referees, Hee-Seung Yang, Youjin Hahn, and the participants at the KDI-3ie Conference on Impact Evaluation in Development Research, Monash Environmental Economics Workshop, and Australasian Development Economics Workshop for their helpful comments. This paper was previously circulated as "Fishing Ban." All errors are mine. Disclosure: I do not have significant competing financial, professional, or personal interests that might have influenced the work described in this manuscript.

# 1 Introduction

Fisheries and aquaculture provide livelihoods for 10–12 percent of the world’s population (U.N. Food and Agriculture Organization, 2014).<sup>1</sup> In 2014, the sector directly employed 38 million people, with 80 percent of motorized fishing vessels concentrated in Asia (U.N. Food and Agriculture Organization, 2016). China, which maintains the world’s largest fishing workforce and fleet, employed 5.75 million fishery workers in 2015, including 3 million traditional fishermen (China Fishery Statistical Year Book, 2016).<sup>2</sup>

Despite the sector’s economic importance, the FAO estimates that 31.4 percent of world fish stocks in 2013 were fished at biologically unsustainable levels. An additional 58.1 percent of stocks were fully exploited, leaving only 10.5 percent underexploited (U.N. Food and Agriculture Organization, 2016). This widespread overexploitation represents a classic example of the tragedy of the commons, where Coasian solutions are infeasible and government intervention becomes necessary. In response, China has implemented the world’s first large-scale seasonal fishing bans, prohibiting commercial fishing in its Exclusive Economic Zone (EEZ) for two to four months each summer. However, given the challenges of ocean surveillance and the typical difficulties in measuring illicit activities, direct evidence on the effectiveness of such fishing regulations remains limited. This paper addresses this gap using novel nighttime satellite imagery data on offshore vessel detection from the new-generation weather satellite program.

Using a regression discontinuity in time (RDiT) design, I estimate that the implementation of fishing bans reduces nighttime boat detections by 73 percent, while the subsequent lifting of bans reverses this decline. I also obtained position data from AIS-equipped vessels, which tend to be larger and account for approximately 86 percent of Chinese vessels 12 meters or longer. Applying a similar RDiT design, I found comparable reductions in the number of vessels operating within China’s EEZ at the onset of fishing bans, with an even larger decrease in total fishing hours. Likewise, there are sharp increases in vessel counts and fishing hours following the lifting of fishing bans.

The enforcement of the fishing bans is by-and-large effective but far from perfect. Although the start of bans leads to substantial reductions in boat detections and fish-

---

<sup>1</sup>Throughout this paper, I use data from the Food and Agriculture Organization (FAO) of the United Nations’ State of World Fisheries and Aquaculture reports, which are considered the authoritative source on global fishing statistics.

<sup>2</sup>In 2015, 20 percent of Chinese fishery workers were women. Throughout this paper, “fishermen” refers to both men and women in the fishery sector.

ing hours, considerable fishing activity persists, as evidenced by nighttime satellite imagery and AIS position data. There is also evidence of increased fishing ban violations later in the ban periods, with both boat counts and fishing efforts gradually rising as the bans progress. Furthermore, areas predicted to be productive for fishing, based on oceanographic variables, show higher boat presence in the later stages of the bans. The difference-in-differences estimates are smaller than the RDiT estimates, suggesting that the local average treatment effects at the onset of fishing bans may be higher than the average treatment effects over a more extended period.

Furthermore, I find no evidence of spatial discontinuity at the Exclusive Economic Zone (EEZ) border during the fishing ban, suggesting imperfect enforcement of territorial fishing rights. Moreover, I find substantial spillover effects of the Chinese fishing bans in neighboring EEZs. The starts of the Chinese fishing bans also reduce the boat detections in bordering EEZs. Similarly, but to a less extent, the lifting of the Chinese fishing bans increase the boat detections in the neighboring water. While the spillovers are unlikely to be driven by larger vessels equipped with AIS devices that broadcast their positions, my findings suggest that the impacts of Chinese fishing bans are not limited to the Chinese EEZs.

This paper contributes to a large literature on the policies for the conservation of the environment and natural resources (see [Cropper and Oates, 1992](#) and [Brown, 2000](#) for a review). To the best of my knowledge, this paper is the first to empirically investigate the effectiveness of the Chinese summer fishing ban, which is the first large-scale regulatory policy for a sustainable fishery in a developing country or in the form of seasonal complete ban on commercial fishing.<sup>3</sup>

The literature on environmental conservation policies has found that subnational inter-jurisdictional spillovers are important in considering a national policy on environmental conservation (see, e.g., [Burgess et al., 2012](#); [Lipscomb and Mobarak, 2016](#)). The literature also documents important spillovers of environmental regulation (and enforcement thereof) across firms ([Chan and Zhou, 2021](#)), and the relocation of economic activities due to environmental regulation ([Walker, 2011](#); [Carruthers and Lamoreaux, 2016](#)).

My findings suggest that, in the context of the sustainable marine fishery, international spillover in regulatory policy also affects the effectiveness of environmental reg-

---

<sup>3</sup>In parallel, unpublished work, [Bos \(2021\)](#) also investigates the Chinese fishing ban using VIIRS VBD and AIS-based data. He similarly finds that the Chinese fishing bans are effective but not perfectly enforced. However, this paper differs in several respects, including the use of RDiT as an empirical approach and the investigation of spatial discontinuities at the EEZ borders.

ulation. My findings echo what [Sigman \(2002\)](#) called international free-riding in regulating pollution of transnational river systems.

This paper also contributes to the growing literature that uses remote sensing data to measure and study environmental conditions and economic activities (see, e.g., [Henderson et al., 2012](#); [Michalopoulos and Papaioannou, 2013](#); [Hodler and Raschky, 2014](#); [Lipscomb and Mobarak, 2016](#); [Chan and Zhou, 2023](#), and [Donaldson and Storeygard, 2016](#) for a review). In particular, [Assunção et al. \(2023\)](#) studied the use of a remote sensing system to monitor and enforce conservation efforts in the Brazilian Amazon, where illegal logging was widespread due to weak institutional protection for the environment. They found that the remote sensing system in Brazil greatly facilitated effective environmental monitoring and regulation enforcement against deforestation. Given that the implementation and enforcement of environmental regulations critically depend on monitoring and measurements ([Lipscomb and Mobarak, 2016](#); [He et al., 2020](#)), the findings in this paper highlight the promising potential of using remote sensing data for enforcing environmental regulations.

[Flückiger and Ludwig \(2015\)](#) and [Axbard \(2016\)](#) found that negative income shocks from fishery increase piracy, which induced violence and substantial welfare losses, including by interrupting shipping routes ([Besley et al., 2015](#)). In light of these studies, our findings suggest that fishing bans may have both short-run and long-run effects on piracy across regions.

The remainder of the paper proceeds as follows. Section 2 provides institutional background on seasonal fishing ban policies. Section 4 presents evidence on the effectiveness of Chinese fishing bans. Section 5 examines patterns of ban violation. Section 6 documents evidence of EEZ incursions and regulatory spillovers. Section 3.5 analyzes fishing effort using AIS-based measures and discusses measurement considerations. Section 8 concludes.

## 2 Background

### 2.1 Fishing Ban: Why?

China's fishery sector has expanded dramatically since market reforms began in the late 1970s. By 2016, China had become the world's largest fishing nation, with approximately 20 million people dependent on fisheries for their livelihood and 14 million workers employed in the sector either directly or indirectly ([China Fishery Statistical](#)

[Year Book, 2016](#)). The nation's fishing fleet comprised over one million vessels, with two-thirds being motorized. Of the 272,000 motorized vessels operating at sea, 69 percent were small-scale vessels under 12 meters in length (Table 1).

While total marine catches increases by many folds since the Economic Reform, many fish stocks declined quickly. In the 1980s and early 1990s, China implemented a number fishery management policy, including a fishing vessel registration and licensing system and resource fee collection scheme. However, these measures did not seem adequate. Starting from the mid-1990s, China has imposed a seasonal fishing ban, along with other policies aiming at reducing the capacity of fishing fleets.<sup>4</sup>

Table 1: Number of Seafaring Fishing Vessels by Size

	Number		Tonnage	
Less than 12 meter	186,781	68.6%	882,361	10.0%
12 meter to 24 meter	49,697	18.2%	1,919,347	21.8%
24 meter or longer	35,844	13.2%	5,989,801	68.1%
Total	272,322	100%	13.838,949	100%

Notes: Data as of the end of 2015 from the [China Fishery Statistical Year Book \(2016\)](#).

## 2.2 Fishing Ban: When?

China first officially introduced a seasonal fishing ban or moratorium in the Yellow Sea and the East China Sea in 1995. In 1999, the summer fishing ban was extended to the South China Sea, covering most of China's marginal seas in the Pacific. In 2009, the Chinese Ministry of Agriculture further extended the duration of summer fishing ban. The duration of the annual fishing ban varies for different marine areas. But most recently in 2017, the Ministry of Agriculture synchronize the starting date of the annual fishing ban to an early date of May 1st, while leaving the ban period to end at different dates for different marine zones.

As detailed in the following section, we focus on the sample period from 2012 to 2017 due to data availability. Table 2 displays the effective dates of annual fishing bans

---

<sup>4</sup>It should be noted that many have argued that official statistics of marine catches have been mis-reported. In particular, marine catches had been over-reported since the mid-1990s ([Watson and Pauly, 2001](#)), which suggested that the over-fishing and collapsing speed of fishery stock in Chinese EEZ may be underestimated based on reported marine catches. Indeed, FAO has treated the Chinese fishery statistics with caution and separated them from those from the rest of world ([FAO, 2002](#)).

from 2009 to 2017 for various Chinese marine zones. Prior to 2017, the duration of fishing bans ranged from 2.5 to 3.5 months. Since 2017, the fishing bans in each zone have been expanded, now ranging from 3.5 to 4.5 months during the summers, representing the most extensive bans since their introduction in 1995.

### 2.3 Fishing Ban: Where?

According to the United Nations Convention on the Law of the Sea, China has sovereign rights to the marine resources below the surface of the sea within its Exclusive Economic Zones (EEZs). An EEZ covers the sea zone from the coastal baseline to 200 nautical miles outward (approximately 370.4 kilometers or 230 miles) unless it overlaps with a 200-nautical mile zone of another nation. In such cases, conventionally, the midpoints of the maritime areas between two nations' coastal baselines determine the outward boundary of an EEZ. China's fishing bans, therefore, apply to its EEZs.

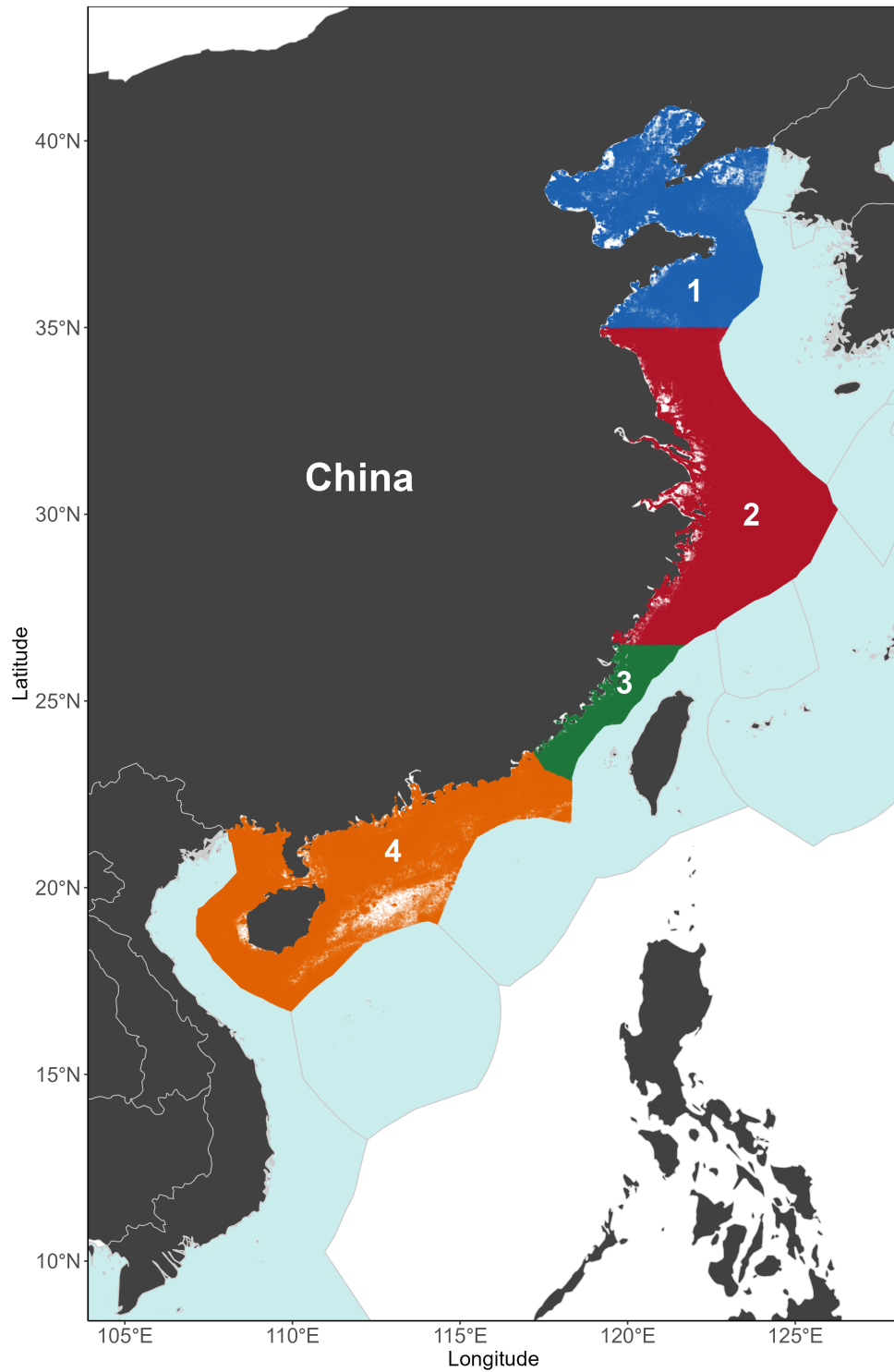
In Figure 1, I plot the EEZs for each marine zone with fishing bans as listed in Table 2. The Paracel Islands in the South China Sea are controlled and claimed by China, but their sovereignty is disputed by the governments of Vietnam and Taiwan. The Spratly Islands are claimed by China, Indonesia, Malaysia, the Philippines, Taiwan, and Vietnam. All of these governments, except Indonesia, also control parts of the Spratly Islands. China's maritime claims in the South China Sea further conflict with those of Brunei. Additionally, China, Taiwan, and Japan claim uninhabited islands respectively named Diaoyudao Islands, Diaoyutai Islands, and Senkaku Islands. These disputed islands are located to the northeast of Taiwan and to the west of Okinawa Island.

Table 2: Effective Dates of Fishing Bans

Zone Number	Zone Description	Years 2009 – 2016			Year 2017 onward		
		Start Date	End Date	Start Date	End Date		
1	Northern Yellow Sea (North of N 35°)	June 1st	September 1st	May 1st	September 1st		
2	Southern Yellow Sea and Northern East China Sea (between N 35° and N 26°30')	June 1st	September 16th	May 1st	September 16th		
3	Southern East China Sea (between N 26°30' and Min-Yue marine boundary)	May 16th	August 1st	May 1st	August 16th		
4	Taiwan Strait and South China Sea (between Min-Yue maritime boundary and N 12°)	May 16th	August 1st	May 1st	August 16th		

Notes: This table lists the start and end dates of fishing bans in each zone for different years. In descending order from the north, Zone 1 is the northernmost, and Zone 4 is the southernmost. The text in each zone corresponds to the same color coding as shown on the map in Figure 1, which illustrates the geographic extents of these zones in our analysis. There were minor exceptions in Zones 2 and 3 regarding certain fishing methods.

Figure 1: Chinese EEZ, Fishery Regulatory Zones, and Neighboring EEZs



This map shows China's four fishery regulatory zones within its EEZ (Zones 1-4, colored), along with neighboring countries' EEZs and disputed areas (light blue). EEZ boundaries are from Marine Regions' World EEZ Version 8.

Due to the complications arising from these sovereignty disputes, I have excluded the EEZs claimed by China that are derived from the sovereignty of these disputed islands in my analysis in this paper. Moreover, I have also excluded the EEZs claimed by China that are derived from islands controlled by the Taiwan authorities. Throughout this paper, I refer to Taiwan as a geographic area or its government without implying any particular legal status. Similarly, I refer to China as the authority of the People's Republic of China (P.R.C.) or as a geographic area where the P.R.C. maintains effective and undisputed control.

I obtained Geographic Information Systems (GIS) data from the Marine Regions organization, using the Version 8 World EEZ Boundaries dataset published in 2014. Based on this boundary data, Figure 1 illustrates the undisputed and disputed EEZs of China and its neighboring countries in the Northwest Pacific Ocean.

## 2.4 Fishing Ban: How?

The vastness of the ocean poses significant challenges to the effective enforcement of fishing bans. During ban periods, the China Coast Guard, in coordination with provincial fisheries ministries, undertakes patrols and inspections of fishing vessels to ensure compliance. Violations of these bans are subject to prosecution. For example, in 2017, Chinese authorities conducted patrols spanning over 800,000 nautical miles, inspected approximately 76,000 fishing vessels, issued fines for 2,764 fishing ban violations (including over 100 criminal prosecutions), and confiscated 800 tons of fish along with 89,000 meters of fishing nets ([Ministry of Agriculture, 2017](#)).

To regulate fishing capacity, China adopted a zero-growth policy in 1999, accompanied by a strict vessel licensing policy. During fishing ban periods, fishery authorities inspect ports to identify unregistered vessels and detect fishing ban violations among both registered and unregistered vessels. In certain regions, fishermen are also required to surrender their fishing equipment during the ban period. To offset income losses during these bans, the Chinese government has recently introduced modest subsidies for fishermen.

### 3 Data Description

#### 3.1 VIIRS Boat Detection Data

The primary dataset used in this paper is the VIIRS Boat Detection (VBD) data, provided by the National Oceanic and Atmospheric Administration (NOAA). The VBD project, jointly sponsored by NOAA and the U.S. Agency for International Development, utilizes remote sensing imagery from the Suomi National Polar-orbiting Partnership satellite.

NOAA, in collaboration with the National Atmospheric Administration, developed the Joint Polar Satellite System (JPSS), a next-generation polar-orbiting operational environmental satellite program in the U.S. Launched in 2011, JPSS is intended to replace the U.S. Air Force's Defense Meteorological Satellite Program (DMSP), with the Suomi NPP as the program's first satellite. The second satellite, JPSS-1, was launched in November 2017.

Most prior economic studies using remote sensing data have relied on imagery from the DMSP-OLS program.<sup>5</sup>

The VIIRS Boat Detection data are derived from images captured by the Visible Infrared Imaging Radiometer Suite (VIIRS), the primary imaging instrument on the Suomi NPP satellite. Compared to the imaging sensors in the DMSP Operational Linescan System (DMSP-OLS), VIIRS provides superior remote sensing imagery, offering higher spatial resolution and an enhanced ability to detect faint light sources. Specifically, nighttime DMSP-OLS pixels cover a  $5 \text{ km} \times 5 \text{ km}$  area, while the VIIRS Day/Night Band (DNB) sensor captures a finer  $742 \text{ m} \times 742 \text{ m}$  footprint. The low-light imaging detection limit is approximately  $5 \times 10^{-10} \text{ Watts/cm}^2/\text{sr}$  for DMSP-OLS, compared to  $2 \times 10^{-11} \text{ Watts/cm}^2/\text{sr}$  for VIIRS. In summary, the VIIRS DNB offers roughly 45 times finer spatial resolution and is 25 times more sensitive in low-light imaging than DMSP-OLS ([Elvidge et al., 2013](#)).

In addition, as its name suggests, VIIRS can capture both imagery and radiometric measurements across the visible and infrared bands of the electromagnetic spectrum. This capability allows for distinguishing light from human activities, such as fishing vessels and LED lighting, from other sources like gas flares at oil fields or explosions in conflict zones ([Elvidge et al., 2015b](#)).

Since 2000, fishery agencies in Japan, Korea, Thailand, and Peru have received per-

---

<sup>5</sup>See [Donaldson and Storeygard \(2016\)](#) for a review of this literature.

mission to use DMSP-OLS data for fishery management, albeit with a minimum three-hour delay. However, DMSP-OLS's limited capacity for low-light detection at fine spatial resolutions, coupled with the lack of automated boat detection algorithms, has restricted its utility for fishery management applications. The VIIRS Boat Detection project has significantly enhanced satellite imagery's role in fishery management by developing an automated boat identification system using VIIRS DNB images, which rely on sensors adapted to a broad wavelength spectrum.

In a nutshell, the VBD algorithm detects spikes in illumination from offshore areas in the DNB images while controlling background noise radiance caused by moonlight. It also filters out recurring light sources (such as features on land) and energetic particles in the upper atmosphere (ionosphere) that can affect electromagnetic sensors. The algorithm further classifies boat detections as either strong or weak by comparing the spikes to neighboring pixels. Additionally, it uses the spectral characteristics of a spike to identify and label gas flares, such as those from offshore drilling stations. For more in-depth information about the algorithms, please refer to [Elvidge et al. \(2015a\)](#), which also includes a validation study demonstrating that the algorithm correctly identified 99.3% of the reference pixels. These reference pixels were chosen from a set of 594 boats visually identified by an analyst and an additional 245 pixels that were not initially identified by the analyst.

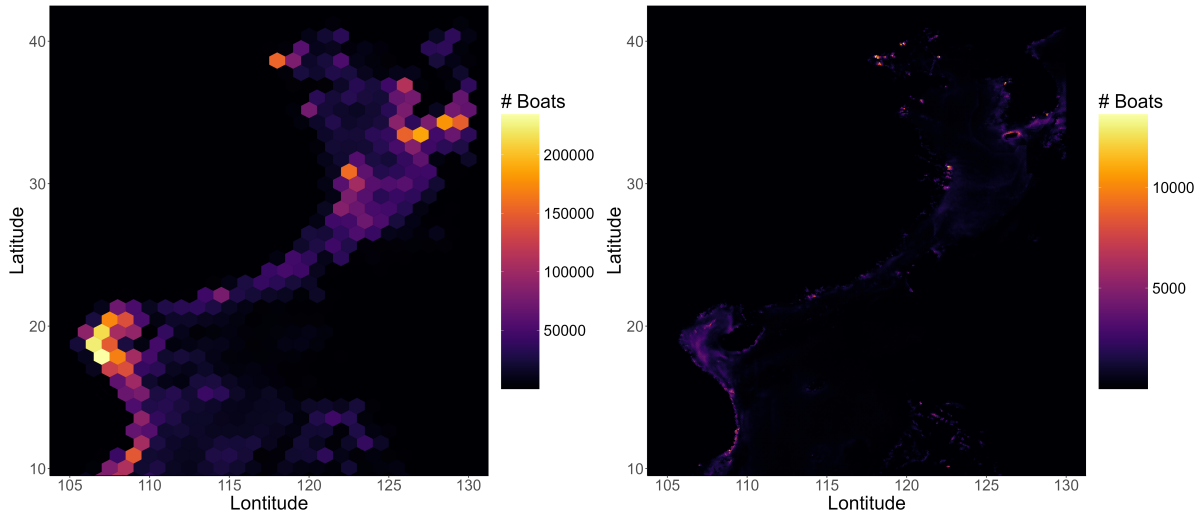
Given that the boat detection is a product of remote sensing imagery, the ability to detect boats is considerably affected by the prevailing weather in a location. Although the algorithm adopted a sharpness index to rate the sharpness of features and identify detection that is affected by clouds, dense clouds, rains, and storms limit the ability for the remote sensing to capture night light and hence detect light emitted by boats. Moreover, the sensors and algorithm are most capable of detecting offshore boats at night with new moon, where the oceans are less lit by moonlight. In full moon nights, the algorithm could have false identifications of boats due to the brightness variations in clouds.

However, despite its limitations, the VBD data offers a unique dataset of offshore boats at a high frequency across an extensive spatial scale. The VBD data is available for most Exclusive Economic Zones (EEZs) in Asia, Oceania, North America, and select European countries. Notably, the VBD data covers all of China and its neighboring countries' EEZs. Since the Suomi NPP scans the same location twice, once around noon and again around 1:30 AM local time, the VBD data provides daily (nightly) boat identifications at a fine spatial resolution across a vast geographic area.

### 3.2 Boats at Night

The VBD data analyzed here cover the period from April 2, 2012, to December 31, 2017. The sample includes both strong and weak boat detections while excluding blurry detections, gas flares, glows, recurring lights, and offshore platforms. Figure 2 displays two heatmaps illustrating the spatial density of aggregated boat detections over the sample period. Both maps cover the same geographic region, encompassing China's EEZ and adjacent waters. The left panel employs a spatial resolution of one degree latitude and longitude, equivalent to approximately 110 kilometers north-south and 100 kilometers east-west.<sup>6</sup>

Figure 2: Boats at Night



Notes: Each hexagonal area in the heatmap above is color-coded to indicate the total number of boat detections from April 2, 2012, to December 31, 2017. The geographic extent is defined by longitude (E) on the horizontal axis and latitude (N) on the vertical axis. In the left subplot, each hexagon spans 1 degree in both latitude and longitude, approximately equivalent to 100 km (or 60 miles). In the right subplot, each hexagon covers 0.1 degree in both directions, roughly 10 km.

As shown in the left subplot of Figure 2, marine areas near the shore are generally brighter than international waters or distant EEZs. The brightest regions, indicating the densest concentrations of detected boats, are near the shores of Beijing, Tianjin, Shanghai, Hong Kong, and Guangzhou—China's largest cities. Each hexagonal cell in the heatmap covers approximately 7,100 km<sup>2</sup>. In the areas with the highest boat density,

<sup>6</sup>1 km is approximately 0.621 miles, and 1 mile is approximately 1.609 km; 1 nautical mile is 1.852 km.

there are up to 200,000 detections per cell, equating to nearly 28 detections per square kilometer over 4.75 years.

The right subplot of Figure 2 presents a similar heatmap with a finer spatial resolution. Here, each hexagon spans 0.1 degrees of latitude and longitude, covering an area of approximately 71 km<sup>2</sup>. Densest areas record up to 10,000 detections per cell, or close to 140 detections per square kilometer over 4.75 years. Additionally, several bright spots are visible near the Shandong Peninsula, which is surrounded by the Yellow Sea in eastern China around N 37°, and near the Liaodong Peninsula, also bordered by the Yellow Sea in northern China around N 40°.

Overall, coastal areas exhibit higher densities of boat detections, consistent with previous studies using Automatic Identification System (AIS) data to map fishing activity distributions in Chinese waters (Yan et al., 2022).

Outside China's EEZ, significant boat detection activity is visible near the southern Korean Peninsula, particularly around Jeju Island, the largest island of South Korea. The marine area off Vietnam's coast also shows a notable band of detections, aligning with the known overfishing pressures in this region (U.N. Food and Agriculture Organization, 2014). Figure 2 highlights substantial spatial variation in fishing intensities, with certain regions clearly serving as primary fishing grounds.

### 3.3 Cloud Cover

Since cloud cover limits a satellite remote sensor's ability to detect light and, consequently, boats at night, accounting for cloud cover in an ocean area allows for more accurate estimates of nighttime boat detection. I obtained global cloud cover images from the Earth Observation Group at the Payne Institute for Public Policy, Colorado School of Mines.<sup>7</sup> The nightly cloud cover data, derived from the VIIRS cloud mask, have a spatial resolution of 15 arc seconds, or approximately 500 meters at the Equator. These data indicate whether a given pixel is cloud-covered. Together with the nightly VIIRS DNB imagery mosaic, the cloud cover mask served as input for the VIIRS Boat Detection (VBD) algorithms and outputs discussed in the previous section. For further details on VIIRS nightlight products, see Elvidge et al. (2013, 2017).

I aggregate pixels within a regulatory zone in China's EEZ to calculate the proportion of pixels covered by clouds on a given night when the Suomi NPP satellite scans a geographic area.

---

<sup>7</sup><https://payneinstitute.mines.edu/eog/>

### 3.4 NASA Ocean Color

Oceanographic conditions have been shown to influence the economic returns of marine fishing (see, e.g., [Flückiger and Ludwig, 2015](#); [Axbard, 2016](#) and references therein). Satellite-based remote sensing offers opportunities to monitor global oceanographic conditions with fine spatial resolution and high temporal frequency. NASA's Ocean Biology Processing Group collects and processes satellite imagery, providing these data products through the Ocean Color platform.

The color of the ocean is influenced by the interaction of sunlight with microscopic particles within the water, including phytoplankton, minerals, and organic matter. The absorption and scattering of different light wavelengths by these materials determine the ocean's perceived color.

Phytoplankton, a crucial component of marine ecosystems, form the base of the oceanic food web and are the primary food source for small pelagic fish essential to human diets. These microscopic, single-celled plants use chlorophyll-a for photosynthesis, similar to terrestrial plants. Consequently, productive waters rich in phytoplankton generally appear green due to chlorophyll-a, while less productive waters appear blue.

Scientists can estimate phytoplankton concentrations by measuring chlorophyll-a levels via satellite data. This information offers insights into the distribution and abundance of phytoplankton, providing a valuable indicator of marine ecosystem health and productivity.

I obtained data on the concentration of the photosynthetic pigment chlorophyll-a in near-surface ocean water from NASA's Ocean Color.<sup>8</sup> Chlorophyll-a concentration, measured in  $mg/m^3$ , is calculated using empirical relationships between field-measured chlorophyll-a levels and spectral remote sensing reflectances (Rrs). This calculation requires three or more spectral bands spanning the 440–670 nm range, which the VIIRS sensor satisfies ([Hu et al., 2019](#)). Chlorophyll-a concentration data are available at a daily frequency throughout the sample period, with a spatial resolution of 9 km × 9 km.

I also obtained sea surface temperature data from NASA's Ocean Color. These measurements, derived similarly from VIIRS imagery, are available at the same temporal frequency and spatial resolution. These two variables provide valuable information on the biological productivity of marine areas.

---

<sup>8</sup><https://oceancolor.gsfc.nasa.gov/>

### 3.5 AIS-based Measures of Fishing Activities

To measure apparent fishing effort, Global Fishing Watch uses data from the Automatic Identification System (AIS)—a vessel tracking system originally designed for collision avoidance—and applies machine learning techniques to detect fishing vessels and activities.

Specifically, [Kroodsma et al. \(2018\)](#) trained two convolutional neural networks (CNNs). One CNN classifies fishing vessels by learning the characteristics of fishing and non-fishing vessels from official fleet registries. The other CNN detects fishing activities by analyzing 22 billion global AIS positions from 2012 to 2016. AIS devices broadcast a ship’s identity, position, speed, and turning angle every few seconds. This information is instrumental in inferring fishing activities; for example, trawlers typically travel at much lower speeds while fishing compared to when they are in transit, resulting in a bimodal speed distribution for trawlers ([Yan et al., 2022](#)).

Using updated AIS algorithms, neural network models, and a comprehensive vessel registry database, Global Fishing Watch provides a dataset on global marine fishing effort from 2012 to 2020. This dataset, which I obtained from Global Fishing Watch, is available at the vessel level with a spatial resolution of 0.1 degrees. It monitors over 100,000 unique fishing vessels, with approximately 70,000 active annually. I observe the number of active fishing vessels in each 0.1-degree geographic grid cell daily, along with their fishing hours within these cells.

In Section 7.1, I aggregate the number of fishing vessels and their fishing hours to the level of regulatory zones. This dataset offers valuable insights into the intensity of fishing activities that may not be fully captured by nighttime boat detections alone. Moreover, since the dataset includes the registration country of each vessel, it enables an analysis of fishing activities within an EEZ and the specific countries involved.

A limitation of AIS data is that AIS devices can be turned off to evade monitoring, particularly during potentially illegal fishing activities. To examine the extent to which AIS-disabling behaviors might impact our previous AIS-based analysis, I obtained a dataset of AIS-disabling events from Global Fishing Watch. Using machine learning techniques, [Welch et al. \(2022\)](#) derived data on AIS (Automatic Identification System) disabling events from Global Fishing Watch’s AIS dataset, which includes over 3.7 billion AIS messages from fishing vessels between 2017 and 2019. They developed a rule-based classification model to identify gaps in AIS transmissions likely caused by intentional disabling.

The resulting dataset, limited to waters more than 50 nautical miles from shore to minimize noise from technical issues, revealed over 55,000 suspected disabling events. Importantly, this dataset captures disabling events only from vessels that broadcast AIS at some point, representing a subset of global fishing activity. The dataset provides details for each suspected disabling event, including location, time, duration, and vessel characteristics (flag state, gear type, length, and tonnage).

## 4 Fishing Bans and Boat Detections

This section employs two empirical approaches to evaluate the impact of China's summer fishing bans on boat detections in Chinese Exclusive Economic Zones (EEZs). The first approach is a regression discontinuity in time (RDiT) design. The second approach is a difference-in-differences design.

### 4.1 Parametric Estimation with RDiT Design

The RDiT design exploits time-series variation in fishing ban policies across regulatory zones. To implement the RDiT design both parametrically and nonparametrically, I first aggregate nightly boat detections within each regulatory zone, as shown in Figure 2 and detailed in Table 2.

The parametric approach controls for seasonal variations through a polynomial specification and estimates ban effects using a binary treatment indicator. The nonparametric approach implements the RDiT design using local polynomial estimation.

For each zone  $z$ , I estimate:

$$Y_{zt} = \gamma_z B_{zt} + f_z(t) + \delta'_z X_t + \epsilon_{zt} \quad (1)$$

where  $Y_{zt}$  is the log number of boat detections in zone  $z$  on night  $t$ ;  $B_{zt}$  indicates whether a fishing ban is effective;  $f_z(t)$  is a polynomial in day of year (1-366);  $X_t$  is a vector of controls; and  $\epsilon_{zt}$  is the error term. The coefficients  $\gamma_z$  and  $\delta_z$  are zone-specific.

Table 3 presents estimates of  $\gamma_z$  by zone. Columns (1) and (2) focus on the onset of fishing bans, excluding post-ban observations. Columns (3) and (4) examine ban lifting, excluding pre-ban observations. For expositional clarity and to economize on space, I maintain a consistent treatment indicator that equals one during active bans across all specifications, rather than using separate indicators for ban implementation

and lifting.

All specifications include a quadratic time polynomial to capture seasonal patterns. Columns (2) and (4) additionally control for cloud cover, day-of-week fixed effects, and lunar day-of-month fixed effects. These controls account for systematic variation in fishing activity due to work schedules and measurement challenges from cloud cover and lunar reflections affecting satellite detection capabilities.

Standard errors, reported in parentheses, are robust to heteroskedasticity and autocorrelation following [Newey and West \(1986\)](#), allowing for serial correlation up to 35 nights.

[Table 3](#) reveals that summer fishing bans significantly reduced boat detections across most regulatory zones. In Zone 1, the fishing ban decreased boat detections by 51.0 to 86.9 log points across specifications, with all estimates significant at the 1% level. The effects are particularly pronounced when the ban is first implemented (columns 1-2), showing reductions of 69.5 to 86.9 log points.

In Zone 2, the ban's impact exhibits substantial temporal variation. When the ban begins (columns 1-2), it reduces boat detections by 100.7 to 128.2 log points, with estimates significant at the 1% level. However, estimates from the ban-lifting sample (columns 3-4) are economically small and statistically insignificant.

Zone 3 exhibits consistent negative effects across specifications, ranging from 29.9 to 87.8 log points. The estimates are statistically significant at the 1% level when the ban begins (columns 1-2) and at the 5% level immediately following implementation (column 3), though the effect becomes insignificant with full controls after the ban's lifting (column 4).

The ban's impact is most consistent in Zone 4, with all specifications showing significant reductions at the 1% level. The effects range from 54.2 to 108.8 log points, suggesting substantial decreases in fishing activity throughout the ban period.

Overall, the starts of fishing bans have large, negative, and statistically significant impacts at the 1% level on boat detections across all regulatory zones and specifications. Dependent on specifications and specific zone, the start of fishing bans reduces boat detection by 50% to 72%. The ends of fishing bans have the opposite effects, but the magnitudes and precision of estimates are more muted. The positive effect of the ending of fishing bans on boat detections range from null for Zone 2 in one specification to 225%

Table 3: Fishing Ban and the Number of Boats Detected: RDiT Estimates by Zone

	Ban ON		Ban OFF	
	(1)	(2)	(3)	(4)
Zone 1				
Fishing Ban Effective	-0.869*** (0.246)	-0.695*** (0.173)	-0.810*** (0.206)	-0.510*** (0.117)
Obs.	1330	1330	1261	1261
Zone 2				
Fishing Ban Effective	-1.282*** (0.252)	-1.007*** (0.127)	0.003 (0.317)	0.145 (0.156)
Obs.	1401	1401	1262	1262
Zone 3				
Fishing Ban Effective	-0.878*** (0.320)	-0.783*** (0.220)	-0.567** (0.262)	-0.299 (0.223)
Obs.	900	900	1180	1180
Zone 4				
Fishing Ban Effective	-1.088*** (0.292)	-0.753*** (0.162)	-0.746*** (0.162)	-0.542*** (0.163)
Obs.	1160	1160	1350	1350
Sample	Days before a fishing ban's lifting		Days after a fishing ban becoming effective	
Day of the Year	Quadratic	Quadratic	Quadratic	Quadratic
Day of the Week F.E.	-	X	-	X
Day of the Lunar Month F.E.	-	X	-	X
Share of Cloudy Pixels	-	X	-	X

Notes: This table reports the parametric estimates of fish ban on the log number of boat detections. Panels 1 to 4 from the top represent estimates for Zones 1 to 4 respectively. Each regulatory zone has one fishing ban each year over the sample period from 2012 to 2017. The specifications in Columns (1) and (3) include a quadratic term of the day of the year to control for seasonal effects. The specifications in Columns (2) and (4) additionally include day of the week indicators, day of the lunar month indicators, and the share of cloudy pixels in a regulatory zone in a night. Columns (1) and (2) exploit the discontinuity in time when fishing bans become effective, and therefore drop observations after the fishing bans were lifted in the later part of the year. Columns (3) and (4) exploit the discontinuity in time when fishing bans were lifted by dropping the observations before the fishing bans became effective in the early part of the year. In all columns, "Fishing Ban Effective" is a binary variable that equals one if a fishing ban is in effect on that day and zero otherwise. Newey and West (1986) heteroskedasticity-and-autocorrelation robust standard errors are reported in the parentheses, where the maximum lag of serial correlation is 35 nights.

## 4.2 Graphic Representation and Non-parametric Estimation of RDiT

If the parametric specification is correct, the estimates have the advantage of being efficient. The Newey-West standard errors also allow for time-series correlation in the error term for inference. However, if the parametric assumptions are not approximately correct, perhaps due to misspecified polynomials or omitted variables, the estimates may be biased. To address these concerns, I will employ a nonparametric RD in Time design, also known as the interrupted time series method (see [Davis, 2008](#); [Chen and Whalley, 2012](#); [Anderson, 2014](#); [Auffhammer and Kellogg, 2011](#) for examples, or [Hausman and Rapson, 2018](#) for a review of this method). The identification assumption for nonparametric identification with RD in time is that the time trend would move smoothly in the absence of treatments, namely fishing bans in this context.

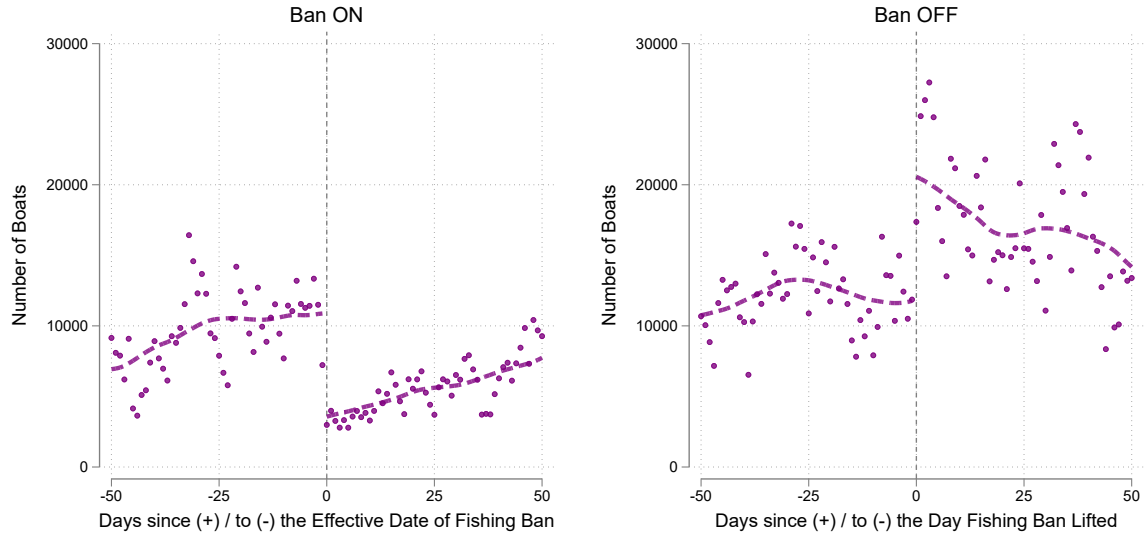
To implement the RD in time design, I separately examine two transitions: when the fishing bans become effective and when they are lifted. Fishing bans during our sample period began and ended at noon. For each regulatory zone and year from 2012 to 2017, I normalize the first night after the ban takes effect to be zero for the ban-switching-on sample. The running variable is defined in non-negative terms as the number of nights since the fishing ban took effect and in negative terms as the number of nights before the fishing ban became effective. Similarly for the ban-switching-off sample, I normalize the first night after the ban lifting to be zero and the running variable is the number of nights since the ban-lifting.

Following the conventional notation, a non-negative running variable indicates the treatment periods. For the ban-on phase, the treatment is the imposition of fishing ban. For the ban-off phase, the treatment is the lifting of the seasonal fishing ban.

I aggregate the total number of boat detections across years by the running variable in nights. I focus on a window where the running variable, denoted as  $\tau$ , falls within the range  $[-50, 50]$ .

To visually assess how the activation of fishing bans affects the number of boat detections, I have plotted the boat detections against the running variables in Figure 3. There are two RD plots in Figure 3. The left plot centers on the start of the fishing ban (Ban ON sample). The right plot center on the ending of the fishing ban (Ban OFF sample). In both plots, I aggregate across the 4 regulatory zone by the value of the running variables.

Figure 3: Boat Detected at Night around the Imposition and Lifting of Fishing Bans



Notes: This figure shows regression discontinuity plots examining nighttime boat detections around China's seasonal fishing ban transitions from 2012-2017. The left panel shows changes when bans begin ("Ban ON"); the right panel shows changes when bans end ("Ban OFF"). Each point represents the total number of boats detected across all regulatory zones, aggregated by the number of nights before/after ban transitions. Day 0 marks the first night following the transition (bans begin/end at noon). The x-axis spans 50 nights before and after transitions. Dashed lines show local polynomial fits on each side of the cutoff. Sample includes four regulatory zones in Chinese waters where seasonal fishing bans are implemented.

The number of boat detections in China's EEZ gradually increases over the 50 days leading up to the commencement of the fishing bans, peaking at around 11,000 detections just a few days before the bans take effect. However, once the fishing bans become active, the number of boat detections experiences a sharp drop to approximately 4,000 in the first night after the fishing ban became effect.

Furthermore, we do not observe substantial increases shortly before the fishing bans become effective, which might be expected if fishermen were intensifying their fishing efforts in anticipation of the bans. The absence of clustering of activity just before the ban effective dates suggests that fishing in the month preceding the bans was likely already at or near full capacity or profit-maximizing intensity. Any further increases in fishing efforts may have been either unfeasible or unprofitable.

We also notice a drop in boat detections one night before the fishing bans. This drop is approximately half the size of the drop observed from two nights before the fishing

ban to the first night of the ban. The decrease in boat detections before the ban suggests that fishing boats had already started returning to their harbors two nights before the fishing bans took effect.

It's important to note that the last observations before the fishing bans were recorded approximately 10.5 hours before the bans became effective, at a time when fishing vessels were required to have returned and docked in the harbors. Considering that a typical fishing cruise covers little more than 10 km per hour and the outer boundary of an EEZ can be up to 370 km offshore, with considerable uncertainties in estimated arrival time due to changing winds and currents, it's not surprising that cautious fishermen would return to the harbor before 1:30 AM on the same day the fishing ban started.

After the initial sharp decline following the implementation of fishing bans, boat detections gradually increase. There are a couple of potential explanations for this trend.

One possibility is that the weather during the ban months becomes progressively clearer, with fewer clouds and less rain, making it easier for satellite imagery and detection algorithms to identify boats at night.

Alternatively, the effectiveness of the fishing bans may erode over time, due to factors on both the demand and supply sides. On the demand side, as the ban period continues, the accumulation of unsatisfied seafood demand may grow, particularly for fresh seafood, as the bans can significantly reduce the seafood supply. Traditional holidays such as the Dragon Boat Festival, Chinese Valentine's Day, and the summer school holiday also fall within the ban period, likely increasing seafood demands.

On the supply side, the potentially higher prices of seafood during the fishing bans could incentivize more fishermen to engage in illegal fishing, especially those facing liquidity constraints and lacking alternative income sources during the bans. Additionally, as fish stocks recover from intensive fishing, the fishing yield for a fixed fishing effort may also increase.

If the fishing bans unraveled completely before their scheduled end date, we wouldn't observe a sharp increase in boat detections when the bans were officially lifted. On the other hand, if the bans remained effective, the incentive to evade the bans and engage in illegal fishing would be highest in the days leading up to their expiration. After a prolonged ban period, fish stocks would be at their peak, and there would be strong demand for seafood. Attempting to fish immediately after the bans were lifted could yield substantial profits (if not detected).

The right subplot of Figure 3 focuses on the lifting of fishing ban. As the bans were

lifted, there was a significant surge in boat detections. The number of detections increased from approximately 12,000 on the eve of the ban lifts to around 25,000 detections two nights after the bans were lifted. Interestingly, the increase on the first night after the ban lift was also roughly half of the drop from the eve of the ban lift to two nights later.

There were no clear upward trends in the nights leading up to the ban lifts, suggesting that illegal fishing might not have been widespread. Furthermore, following the ban lifts, the number of boat detections gradually declined. One possible reason for this decline is that increased fishing activity depleted fish stocks over time, reducing the profitability of fishing and leading to fewer operating fishing boats.

A visual examination of Figure 3 suggests that fishing bans have had a substantial negative impact on boat detections within China's EEZ. However, aggregating across regulatory zones may have obscured significant spatial heterogeneity in the periods leading up to and following fishing ban imposition and lifting, as well as in the effects of the bans themselves. To investigate this potential heterogeneity, I plot similar RD graphs by regulatory zone in Figure 4. As in Figure 3, the RD plots on the left focus on the start of fishing bans, while those on the right focus on the end of the bans. Instead of aggregating across zones in China's EEZ, each row of Figure 4 represents a different regulatory zone.

The disaggregated RD plots reveal substantial heterogeneity in fishing ban compliance across regulatory zones. Zones 1 and 4 exhibit the sharpest discontinuities at ban implementation, with immediate drops of roughly 50 percent in detected vessels. The response to ban lifting is particularly pronounced in Zone 1, where vessel detections surge rapidly. Zone 3 shows more modest discontinuities, suggesting potentially weaker enforcement or different fishing patterns in this region. Zone 4 displays clear but smaller discontinuities compared to Zones 1 and 2, with a notable increase in detection variance after ban lifting.

The first two columns provide estimates of the local average treatment effects (LATEs) of imposing the fishing bans, with the outcome variable as either the number of boat detections or the logarithmic value of boat detections. The last two columns present similar estimates, but this time for the LATEs of lifting the fishing bans.

The RD estimate in the first column suggests that imposing the fishing ban lowered the number of boat detections by 8,228 per night in the Chinese EEZs. The log specification in the second column suggests that this corresponds to a reduction of 129 log points, or 72%, which is a substantial impact.

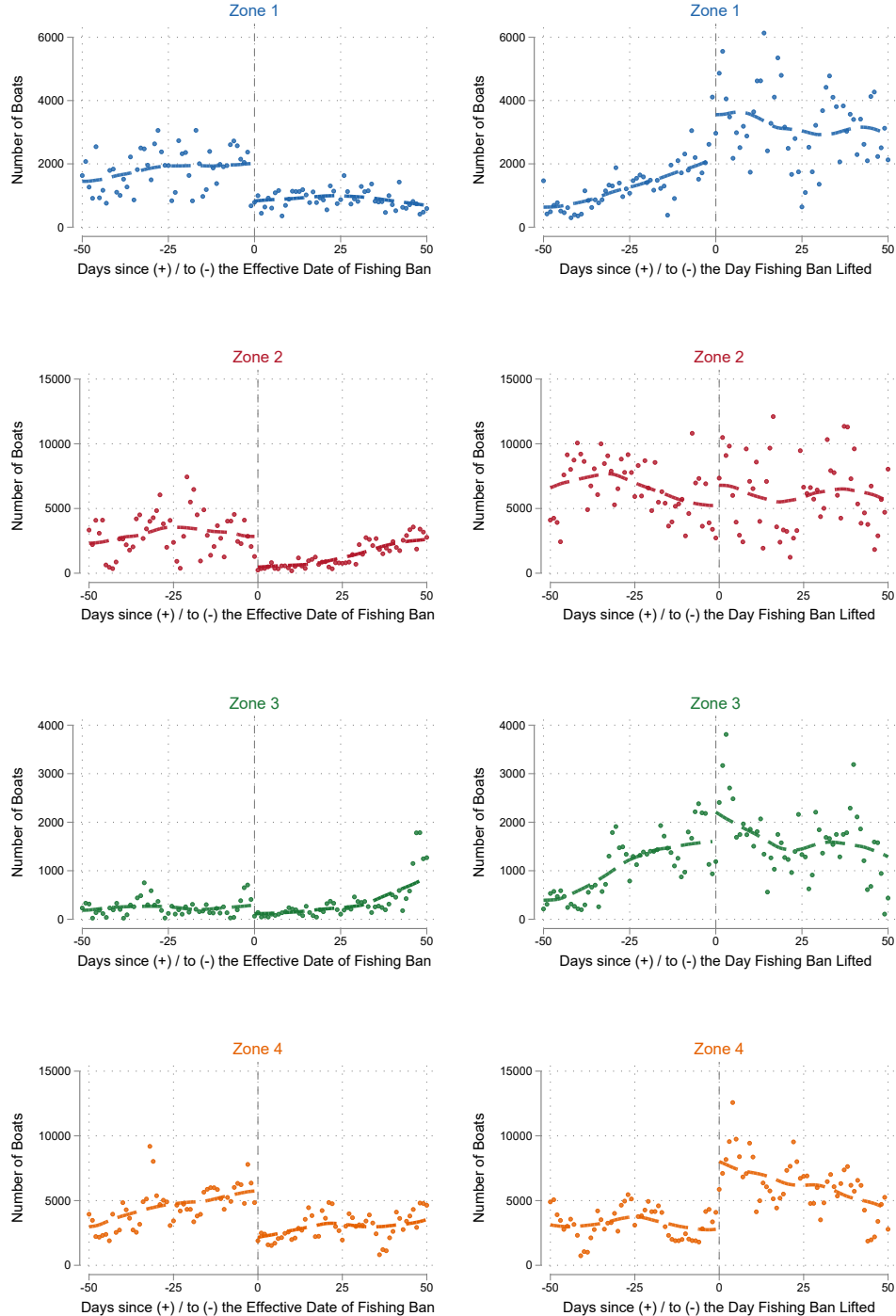
When the fishing bans were lifted, boat detections increased by 10,015 or 57.6 log points, representing a 78% increase. It's worth noting that the LATE estimates for the ban lifting are slightly less precise compared to those for imposition, which is not surprising. As observed in the RD graphs, there is somewhat more noise around the ban lifting compared to ban imposition.

However, all four LATE estimates are highly statistically significant, with each one reaching the 0.001% level of statistical significance.

While fishing bans had an impact on the number of boat detections across the Chinese EEZs, their effectiveness may vary in individual regulatory zones due to differences in local enforcement capabilities or measures. To examine how the fishing bans influenced each regulatory zone, I have presented RD graphs, similar to Figure 3, separately for each zone in Figure 4.

Figure 4 confirms that in each of regulatory zone, the starts of fishing bans substantially reduce the number of boats detected at night, while the ends of bans are accompanied with increases. Comparing the plots on the left to those on the right, we also see that the drops in boat detection around the starts of fishing bans are sharper than those increases around the ends. This pattern echoes the pattern seen in the parametric estimates reported in Table 3. Moreover,

Figure 4: Discontinuity Changes in Boat Detection by Regulatory Zone around Starts and Ends of Fishing Bans



Notes: The RD graphs above are similar to Figure 3 but separately for each zone. The subplots on the left hand side concern the starting of fishing bans; the subplots on the right hand side concern the lifting of fishing bans. Rows 1 to 4 represents Zones 1 to 4 respectively. Each dot represents the number of boat detections across the respective regulatory zone  $\tau$  nights since (+) or before (-) the fishing bans became effective (left subplots) or were lifted (right subplots). Night 0 is the first night after the fishing bans were lifted and the horizontal axis represents  $\tau$ . The vertical axis represents the nightly number of boat detections aggregated over years from 2012 to 2017.

To formally test the statistical significance of the jumps seen in Figure 3 and Figure 4, Table A.1 reports the local polynomial estimates proposed by Calonico et al. (2014). Similar to the parametric estimates in Table 3, Columns (1) and (2) focus on the starts of fishing bans, while Columns (3) and (4) focuses on the endings of fishing bans. Moreover, there are separate panels for each regulatory zone. In addition, the top panel reports estimate on the 4-zone aggregates.

In Columns (2) and (4), the dependent variables are log number of boat detection, similar to Table 3. In Columns (1) and (3), the dependent variables are the absolute number of boat detections.

The nonparametric RD estimates by zone reported in Table A.1 confirm that the starts of fishing bans have large, negative, and statistically significant (at the 1%) on boat detections. In absolute term, the impacts are largest on for Zone 4 in the South China Sea, reducing boat detections by 4,258.

The nonparametric RD estimates reported in the Columns (3) and (4) are all positive and have similar magnitudes to the negative effects of starting the fishing ban in the same zone. However, standard errors of estimates in Column (3), which are about the number of boat detection from the ending of fishing bans tends to be larger than those reported in Column (1), which are about the number of boat detection from the starts of bans. Moreover, the magnitude of the point estimates on the log number of boat detection from the ban-ending sample (column 4) also tend to be smaller than the point estimates from the ban-starting sample (column 2). Overall, these pattern echos that the changes at the beginning of fishing ban are much sharper than the changes around the lifting of those bans.

The nonparametric RD estimates reported in Table A.1 were estimated with the approach by Calonico et al. (2014), which was developed for cross-sectional data. The inference may not be valid in our setting for failing to account for the time-series correlation in the data. I implement a randomization inference procedure (Fisher, 1935). Specifically, for each year in each zone, I randomize the dates when a fishing ban starts or ends. For each simulated switching dates, I create a running variable similar to the one used in the top panel of Table A.1 and estimate a treatment effect for that simulated ban-switching date following the same procedure. I repeat the simulation 1000 times and collect all the placebo treatment effects. Then, I compared the actual estimates reported in the top panel of Table A.1 to the distribution of these placebo estimates. In the left subplot of Figure A.1, the dependent variable is the number of boat detection. In the right subplot, the dependent variable is the log number.

The one-side p-value for the absolute and log specification of the fishing ban estimate is zero around the start of fishing ban. In fact, the estimated effect of ban-start is many times smaller than the smallest placebo estimate among the 1000 simulations, while the estimated effect of ban-lifting is many times larger than the largest placebo estimate. Similarly, the ban-lifting coefficient reported in Column (3) in the top panel of Table A.1 also have a one-side p-value of 0. The ban-lifting coefficient reported in Column (4), where the dependent variable is log number of boat detection, has a p-value of 0.026. The randomization inference exercise supports that statistical significance of our findings reported in both Table 3 and Table A.1.

### 4.3 Validity and Robustness of the RDiT Design

The identification assumption of a sharp RD design rests on that potentially confounding factors change only smoothly at the threshold where the running variable induce sharp change in the treatment variable. Oceanographic Variables may affect fishing activities. I test for the continuity of two oceanographic variables, namely, chlorophyll-a concentration and sea surface temperature, around the starts and ends of China's seasonal fishing bans. As explained in Section 3, I obtained the estimates of chlorophyll-a concentration in upper layers of global ocean and sea surface temperature from NASA Ocean Color. These products are derived from VIIRS images and have  $9 \text{ km} \times 9 \text{ km}$  spatial resolution at daily frequency. I average these high-resolution oceanographic variables to the regulatory zone level for my continuity tests.

In Figure A.2, there are four RD plots related to these two oceanographic variable. The top two plots row is about chlorophyll-a concentration in the upper ocean water. The bottom two plots is about the sea surface temperature. The left two plots center around the starts of fishing bans, while the bottom two plots center around the lifting of those bans.

None of the plots exhibit a discontinuous jump around the cutoff nights. I also test the discontinuity using these oceanographic variable as dependent variable and the same nonparametric estimation procedures. The estimates are annotated in each plot. There are no statistically significant changes in the oceanographic conditions around the changes of fishing bans.

Another potential thread to the validity of a RDiT design is the temporal displacement of fishing activities around the starts and end of the fishing bans. Because the start and end dates of fishing bans were set and announced well in advances, fisher-

men anticipating these policy changes may adjust their fishing activities in responses to changes.

If fishing households, anticipating a shortfall in earnings during the months-long fishing ban, shift a substantial portion of their activities to just before the ban, there would likely be a spike in fishing activity prior to the ban's start, resulting in an upward bias in the RD estimate. In this scenario, the observed reduction in boat detections would exaggerate the fishing ban's effects on fish stock conservation or regeneration.

Conversely, if boats fishing further offshore need to return to port a day early to ensure they anchor in time before the ban begins, this behavior could lead to an underestimation of the fishing ban's impact, as the RD estimate would be biased toward zero.

Indeed, a visual examination of the RD graphs and the previous section's discussion suggest that the number of boats detected may already change one day before the start or end of the fishing bans. This temporal displacement of fishing activities violates the stable unit treatment value assumption.

To address this, I implement a donut hole RD design, as proposed by [Barreca et al. \(2011\)](#). Specifically, I exclude observations within a 7-day window around the first night after the start or end of the fishing bans and re-estimate the effects using the nonparametric estimator of [Calonico et al. \(2014\)](#). Results are presented in Appendix Table A.2, structured similarly to Table A.1.

Compared to the nonparametric estimates from the full sample in Table A.1, the donut hole RD estimates are qualitatively similar and, if anything, show larger magnitudes and statistical significance. This aligns with the visual examination of RD plots in Figure 3 and Figure 4. If there is a change in boat detection the day before a fishing ban starts, it tends to be in the same direction as changes on the first day of the ban, providing no evidence of a surge in fishing activity immediately before the ban.

This lack of intertemporal shifting of fishing activity may not be surprising in the Chinese context. Without refrigeration or other processing, seafood is highly perishable, and there is a strong cultural preference for live and fresh seafood, with frozen and processed products making up a relatively minor share of overall seafood consumption ([FAS Staff, 2021](#)). Furthermore, China is the largest producer of both freshwater and marine aquaculture products ([U.N. Food and Agriculture Organization, 2016](#)), meaning that frozen marine catches compete with not only imported frozen seafood but also domestic fresh aquaculture and wild freshwater products.

Beyond limited demand-side incentives, supply constraints in fishery production

may also restrict intertemporal shifting of fishing activities. Global fishery activities display strong seasonality due to variations in biological activity and marine productivity (Kroodsma et al., 2018). Additionally, fuel expenses account for a significant portion of fishing household expenditures. According to the 2019 China Fishery Statistical Yearbook [Ministry of Agriculture and Rural Affairs of the People's Republic of China \(2019\)](#), fuel and ice expenses comprise 20.1% of total operating costs, while labor costs account for 20.4%. Although the report does not distinguish between aquaculture and capture fishery households, aquaculture workers outnumber capture fishery workers 3-to-1, and feed and seed make up 54.4% of total costs, indicating that fuel and ice expenses are likely much higher for traditional fishing households. Given the seasonality of fishing productivity, the capacity constraints of vessels, and high fuel and ice costs, shifting a substantial amount of fishing activity prior to the start of the ban may not be profitable.

#### 4.4 Difference-in-Differences Estimation

While RD designs provide estimates of local average treatment effects (LATEs) around the threshold, these estimates may differ from the average treatment effects (ATEs) over the entire ban period, even in the absence of intertemporal displacement in fishing activity. This divergence could arise from several factors, including seasonal variation in fishing productivity and potential demand accumulation for fresh seafood during prolonged bans, both of which may affect ban enforcement. From a policy perspective focused on sustainable fishery management, understanding both the ATE during the ban period and the optimal ban duration is crucial. To shed light on these issues, I implement a difference-in-differences design that exploits a 2017 policy change in ban timing.

Prior to 2017, fishing bans began on June 1st for Zones 1 and 2, and on May 16th for Zones 3 and 4. Starting in 2017, all zones implemented a uniform ban start date of May 1st. The left panel of Figure A.3 normalizes time relative to May 1st (day zero) and displays the average number of detected boats by year. Post-2017 observations, represented by solid diamonds, show an expected drop at time zero. In contrast, pre-2017 observations, shown by hollow circles, exhibit no comparable decline on May 1st. This placebo test, leveraging the historical variation in start dates, corroborates that the post-2017 reduction in detected vessels is attributable to ban implementation.

The right panel of Figure A.3 presents a similar placebo test examining the extension

of fishing bans in Zones 3 and 4. Before 2017, these zones lifted their bans on August 1st; since 2017, the ending date has shifted to August 16th. Normalizing time relative to August 16th (day zero), the figure plots average boat detections before and after 2017. Post-2017 data, marked by solid yellow diamonds, reveal a sharp increase in detected vessels at day zero. Pre-2017 data, indicated by hollow blue circles, show no comparable discontinuity. This placebo test using the shifted ban ending date further confirms the causal effect of ban termination on vessel activity.

Figure A.3 motivates a difference-in-differences strategy that uses observations from different years but identical calendar dates within zones as controls, thereby accounting for zone-specific seasonality in vessel detection. I implement this strategy using three specifications, with results reported in Table 4. The unit of observation is an EEZ-day, with each regulatory zone in Chinese waters treated as a separate EEZ. While most coastal nations possess a single EEZ, some countries, such as the United States, maintain multiple EEZs (e.g., around Alaska, Hawaii, and along the eastern seaboard). The dependent variable in all specifications is the log number of detected vessels.

Column (1) includes year fixed effects and EEZ-specific month effects. Column (2) incorporates both EEZ-specific year effects and EEZ-specific month fixed effects. Column (3) employs EEZ-specific year fixed effects and EEZ-specific calendar day fixed effects. The key independent variable is a binary indicator for an active fishing ban, which takes a value of one only for the relevant Chinese EEZ zone during ban periods. Identification stems from within-zone variation in ban effective dates across years.

Standard errors are calculated using two approaches. Two-way cluster-robust standard errors, reported in parentheses, allow for arbitrary correlation within an EEZ across dates and within a date across EEZs. Conley (1999) spatial-temporal robust standard errors, reported in brackets, account for spatial correlation up to 1,000 kilometers and temporal correlation up to 35 nights.

The coefficients are statistically significant at the 5% or 1% level across both standard error calculations, with the exception of Column (1)'s estimate, which achieves only 10% significance using two-way cluster-robust standard errors. The estimated effects are generally smaller in magnitude than those reported in Tables 3 and A.1 for ban initiation, consistent with our earlier evidence suggesting more frequent ban violations during the ban period compared to its onset.

Table 4: Difference-in-Differences Estimates of Fishing Ban on Boat Detections

	(1)	(2)	(3)
Fishing Ban Effective	-0.272 (0.139)* [0.111]**	-0.311 (0.139)** [0.122]**	-0.420 (0.125)*** [0.114]***
Fixed Effects			
Year	X		
EEZ × Year		X	X
EEZ × Month	X	X	
EEZ × Month × Day			X
# EEZ Clusters	147	147	147
# Day Clusters	2,644	2,644	2,644
# Obs.	111,977	111,977	111,977

*Notes:* This table reports the estimates of the impact of the fishing ban on the log number of boat detections using three fixed-effects specifications. Each observation represents an EEZ × day, except that each of the four regulatory zones within the Chinese EEZ is treated as if it were its own EEZ. Each regulatory zone in the Chinese EEZ has one fishing ban each year. Over the sample period from 2012 to 2017, the 4 zones in Chinese EEZ collectively have 24 fishing bans with varying duration, as shown in Table 2. The specification in Column (1) includes EEZ-specific month fixed effects. The specification in Column (2) includes both EEZ-specific month fixed effects and EEZ-specific year fixed effects. The specification in Column (3) includes EEZ-specific day-of-the-year fixed effects and EEZ-specific year fixed effects. Two-way cluster-robust standard errors are reported in parentheses, allowing for arbitrary correlation within an EEZ across dates and a date across EEZs. Additionally, Conley (1999) robust standard errors are reported in brackets, accounting for spatial correlation up to 1,000 km and serial correlation up to 35 nights.

\*  $p < 0.10$ ; \*\*  $p < 0.05$ ; \*\*\*  $p < 0.01$ .

## 5 Violation of Fishing Ban

As time past into the fishing ban, the RD plots in Figure 3 and Figure 4 suggest that boat detection seems to increase. One possible reason may be weather. As summer arrives and the night sky gets less cloudy. More nightlight and hence boats are detected. However, in unreported results, even after the share of cloudy sky in each zone is controlled for, there is still an increase of boat detection as time pass by during the fishing ban.

Another possibility is that enforcement abates over time. If internal quotas exist for the Chinese fishery authorities—such as targets for vessel boardings or fines during the ban period—these could initially heighten compliance pressure, contributing to the sharp drop in fishing activity at the start of the ban. However, enforcement may relax as quotas are met or as the ban period progresses, leading fishermen to anticipate reduced inspections over time. This diminished enforcement could explain the gradual increase in fishing hours and vessel counts toward the end of the ban, suggesting that adaptive behavior by fishermen may weaken the ban’s effectiveness over time.

While the Ministry of Agriculture establishes national fishing regulations for China’s EEZ, enforcement is delegated to provincial fishery agencies. These agencies are responsible for implementing various regulations, including seasonal fishing bans. Given China’s decentralized administrative structure, enforcement likely varies substantially across coastal provinces. Although some provinces may maintain internal inspection targets, the limited transparency of Chinese government agencies makes it difficult to verify specific enforcement protocols. When news media sometimes report the number of inspection made by an provincial fishery agency, I have not found any explicit quotas about enforcement, such as number of boats boarded during the ban period.

A third possibility is that the incentives to fish illegally increase as time passes due to both demand and supply factors. As time passes, there may be pended up demand for fresh seafood. Ideally, one would like to have data on the domestic prices of seafood or some measured of unmet demand. However, I have not been able to locate such data. However, Figure A.4 shows that the average import price of frozen fish increase in the summer months and peak in August. To the extent fresh seafood from Chinese EEZ and imported frozen seafood are substitute, the movements of import price provides some circumstantial evidence of unmet demand in fresh seafood.

While fish stock recovery during bans may increase yields per unit of fishing effort,

direct measures of fish stock health or fishing productivity are unavailable.

To examine whether fishing incentives during bans affect vessel detection, I exploit variation in oceanographic conditions, following the approach pioneered by [Flückiger and Ludwig \(2015\)](#) and [Axbard \(2016\)](#). Marine biology and fishery management research indicates that oceanographic conditions, particularly chlorophyll-a concentration and sea surface temperature, influence marine productivity and fish abundance. [Semedi and Hadiyanto \(2013\)](#) document that most marine capture in the Makassar Strait near Indonesia occurs in coastal areas with sea surface temperatures between 26 °C and 30 °C and chlorophyll-a concentrations between 0.3 mg m<sup>-3</sup> and 2.8 mg m<sup>-3</sup>. Using these intervals, [Axbard \(2016\)](#) construct a measure of local fishing conditions as a proxy for fishermen's income opportunities, finding that negative income shocks increase sea piracy in Indonesia.

Following [Axbard \(2016\)](#), I employ remote sensing data on chlorophyll-a concentration and sea surface temperature to construct measures of fishermen's income opportunities, which may affect incentives to violate fishing bans.

However, given the extensive geographic span of the Chinese EEZ and its regulatory zones, a single measure is unlikely to adequately capture fishing conditions throughout the area. [Semedi and Hadiyanto \(2013\)](#) find that sea surface temperature exhibits non-linear correlations with marine catch, and these relationships depend on chlorophyll-a concentration. The relationship between chlorophyll-a concentration and fish abundance may be non-monotonic. For instance, algal blooms, driven by excess nutrients, reduce sunlight penetration and inhibit benthic algal growth, disrupting the benthic food chain. The decomposition of these blooms depletes oxygen, creating hypoxic conditions in bottom waters. Thus, extremely high chlorophyll-a concentrations indicating algal blooms may correlate with adverse conditions for certain marine species ([Chang et al., 2012](#)).

The complex relationships between sea surface temperature, chlorophyll-a concentration, and fish abundance likely vary with location-specific fish stock characteristics, weather, and other oceanographic conditions. No comprehensive study has yet mapped these relationships across the Chinese EEZ.

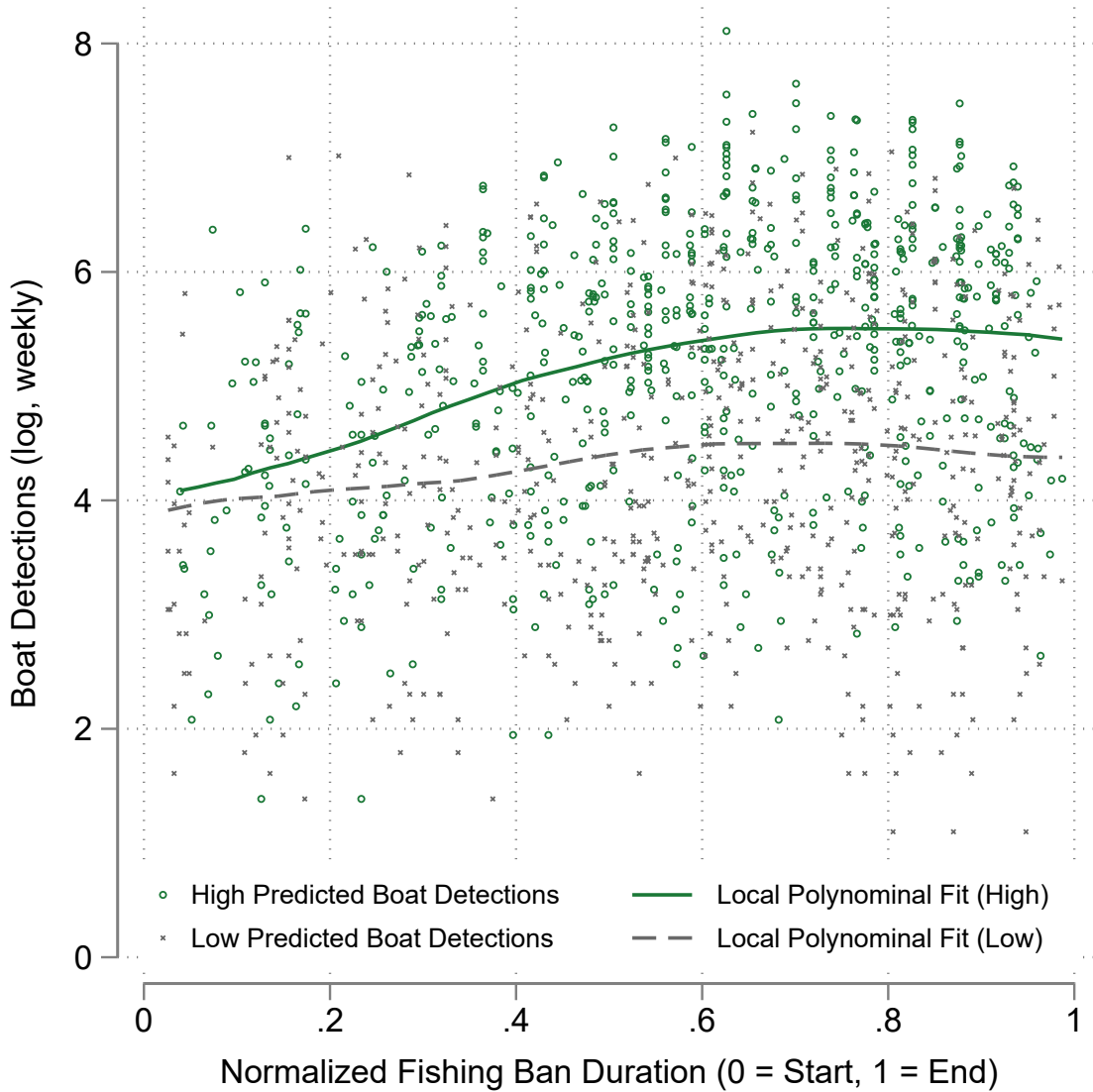
While sea surface temperature and chlorophyll-a concentration vary spatially, they also exhibit substantial seasonal and idiosyncratic variation ([Yu et al., 2019](#)). To predict fishing opportunities, I estimate a LASSO regression ([Tibshirani, 1996](#)) using 1-degree grid data from non-ban periods in the Chinese EEZ and conduct out-of-sample prediction.

Specifically, I aggregate boat detection, average sea surface temperature, and average chlorophyll-a concentration to 1-degree cells at weekly frequencies. The LASSO regression selects predictors from latitude-specific cubic polynomials of mean sea surface temperature, latitude-specific cubic polynomials of mean chlorophyll-a concentration, and polynomials of mean SST and chlorophyll-a concentration up to degree three. The regularization parameter is selected using 10-fold cross-validation exclusively from the no-ban sample. Using the resulting LASSO estimates, I generate out-of-sample predictions of boat detection during ban periods.

To analyze how actual boat detections relate to predictions based on oceanographic conditions, I partition the during-ban sample into above- and below-median predicted boat detections. Given that ban durations vary across zones and years (ranging from 77 to 138 days), I normalize time into the fishing ban by ban length. Figure 5 displays weekly boat detections in 1-degree cells against normalized ban time, separately for cell-week observations with high (above-median) and low (below-median) predicted boat detections based on oceanographic conditions.

While cell-week observations with low predicted boat detections show modest increases in actual detections during ban periods, those predicted to have high boat detections exhibit substantially larger increases. This pattern suggests that favorable oceanographic conditions moderately influence potential illegal fishing during bans, with effects intensifying as the ban progresses.

Figure 5: Boat Detections during Fishing Ban by Oceanographic Conditions



Notes: This figure plots boat detections during fishing bans against normalized ban duration (0 = start of ban, 1 = end of ban), separately for areas with high and low predicted fishing opportunities based on oceanographic conditions. The y-axis shows log weekly boat detections in  $1^\circ \times 1^\circ$  cells. Predictions are generated from a LASSO regression estimated on observations outside of fishing bans between 2012 and 2017, with predictors including flexible latitude-specific polynomials of sea surface temperature and chlorophyll-a concentration. High (low) predicted detections indicate above (below) median predicted values from this model. Green circles and solid line represent areas with high predicted fishing opportunities; gray dots and dashed line show areas with low predicted opportunities. Lines show local polynomial fits.

## 6 EEZ Incursions and Spillover

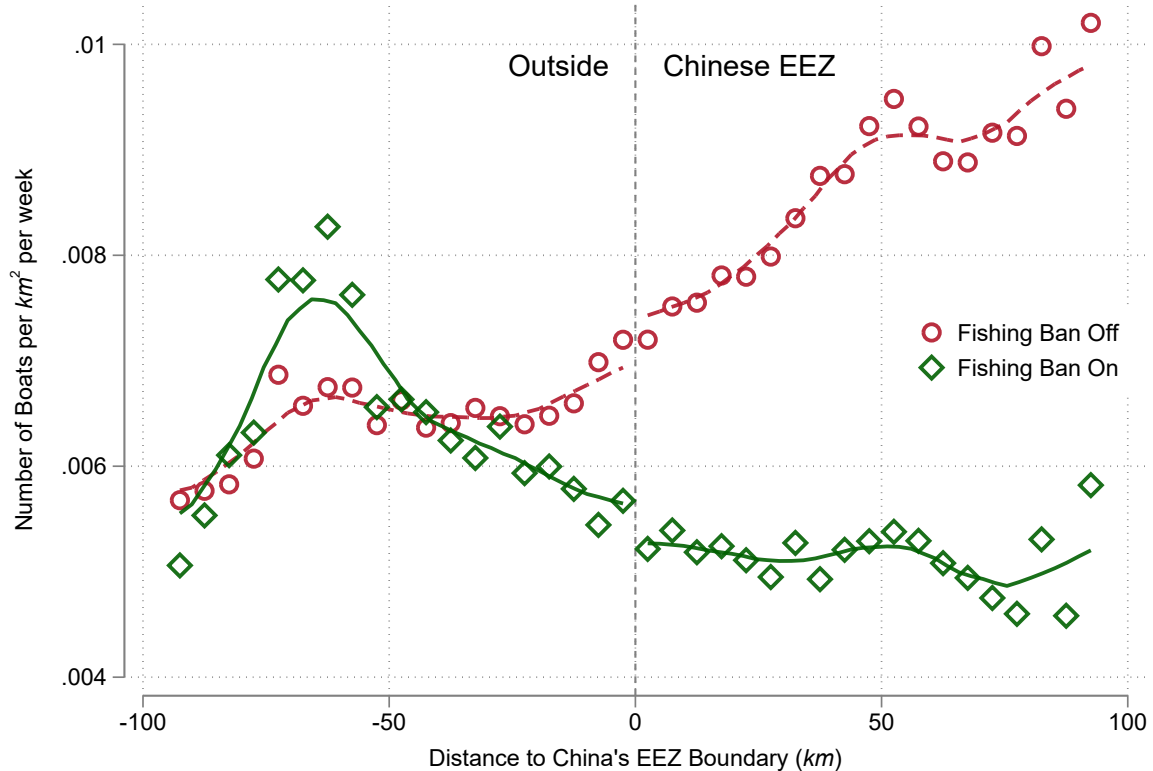
Up to this point, my findings indicate that fishing bans reduce the number of boat detections in the Chinese EEZ. However, it's essential to note that not all boats operating within the Chinese EEZ are necessarily Chinese fishing vessels. Fishing vessels from neighboring countries may engage in illegal fishing within the Chinese EEZ, and conversely, Chinese fishing vessels may operate in the EEZs of neighboring countries.

Countries often have varying preferences for domestic seafood, especially fresh seafood, and their fishing industries can differ significantly in terms of capability and productivity. If EEZ fishing rights are effectively enforced, ensuring that only a country's fishermen exclusively exploit its EEZ, we might observe a discontinuous change in the number of boat detections at the border of two countries' EEZs.

To investigate whether this is the case, I have plotted two spatial RD graphs. In these graphs, the running variable is the distance to the outward boundary of the Chinese EEZ, and the outcome variable is the density of boat detentions.

First, I present a spatial RD graph in Figure 6 for the Chinese EEZ's outward boundary, excluding the China-Vietnam segment. Then, in Figure 7, I present a similar graph but for the China-Vietnam EEZ border.

Figure 6: Boat Density at China's EEZ Boundaries (Excluding China-Vietnam Border)



This figure shows the lack of boat density discontinuities at China's EEZ boundary (excluding China-Vietnam borders) during and outside fishing ban periods. Boat density is measured as detections per  $\text{km}^2$  per week, calculated from  $5 \text{ km} \times 5 \text{ km}$  grid cells. Red circles show average density during non-ban periods; green hollow diamonds show density during ban periods. Each point represents the average density within a  $5 \text{ km} \times 5 \text{ km}$  bin from the EEZ boundary (marked by vertical dashed line at 0), extending to  $\pm 100 \text{ km}$ . Negative distances indicate areas outside Chinese EEZ; positive distances indicate areas inside. Sample includes all available boat detection data, aggregated separately for ban and non-ban periods. Densities are spatially averaged using grid cell centers for distance calculations.

The Gulf of Tonkin, known as Beibu Bay in China, is divided with the Vietnamese EEZ in the west and the Chinese EEZ in the east. Despite the relatively short length of the China-Vietnam EEZ border, this area experiences intense fishing activity, as indicated by Figure 2. Population density is high along the nearby Chinese coasts, and even higher along the Vietnamese coasts. Notably, Hanoi and Hai Phong, the first and third most populous cities in Vietnam, are in close proximity to the Gulf of Tonkin. The average distance between the Vietnamese shore and the Chinese shore in the Gulf of Tonkin is less than 250 km (approximately 155 miles).

As we will see in Figure 6 and Figure 7, an important asymmetry distinguishes these two EEZ boundary segments.

To measure boat density, I aggregate the number of boat detections within a grid composed of numerous  $5 \text{ km} \times 5 \text{ km}$  cells and calculate the number of boat detections per square kilometer per week. I calculate boat density separately for periods when the Chinese fishing bans were effective in the South China Sea and periods when the bans were not in effect. Subsequently, I calculate the distances between the center of each cell and the China-Vietnam EEZ border. Cells are then averaged within distance bins of 5 km.

In Figure 6, the vertical dashed line at zero represents the China-Vietnam EEZ border, projected from a 2-dimensional line onto a 1-dimensional scale. The height of each circle or hollow diamond indicates the average number of boat detections per square kilometer per week. Circles represent detection rates when the Chinese fishing bans were not in effect, while hollow diamonds represent rates during the enforcement of the bans. Each marker reflects the average within a 5-kilometer distance bin, with distance from the border shown on the horizontal axis.

For instance, the first circle to the right of zero represents cells with centers inside the Chinese EEZ, and their distance to the China-Vietnam EEZ border falls between 0 and 5 km. The second circle to the right of the vertical dashed line at zero represents the average boat density rate for cells located 5 km to 10 km away from the China-Vietnam EEZ border, on the side of the Chinese EEZ. The scatter plot extends up to 100 km along the horizontal axis, with each point reflecting a 5-kilometer bin.

Similarly, to the left of the zero dashed line, the horizontal value of a circle or hollow diamond, denoted as  $-x$ , indicates the bin averaging cells whose distance to the China-Vietnam EEZ border falls within the range  $[-x - 2.5, -x + 2.5]$ , for values of  $x$  such as 2.5, 7.5, and so on, up to 97.5.

If we examine the circles in Figure 6, representing boat density during periods when

the fishing bans were not in effect, and the dashed lines, representing their local linear fits, a clear upward gradient becomes evident. This upward gradient suggests that when the fishing bans were lifted, sea areas closer to the Chinese continental shore had more boats detected than areas further away from the shore, and therefore, closer to the outward boundary of the Chinese EEZ.

If we were to extend the horizontal axis of Figure 6, this upward gradient would continue. This gradient confirms that, outside of the China-Vietnam segment, the Chinese EEZ tends to be more densely fished than the other side of the EEZ boundary. Furthermore, areas near the continental shore of China are more densely fished than those further offshore. However, there is no visible discontinuity at the EEZ border when the fishing bans were not in effect.

Examining the hollow diamonds, which represent the periods when fishing bans were in effect inside the Chinese EEZ, reveals no visible discontinuity at the EEZ border either. On the positive domain, i.e., the side of the Chinese EEZ, boat density during the ban periods is significantly lower than that during the no-ban periods within each distance bin. Moreover, there is no apparent upward gradient; if anything, the gradient appears to be slightly downward. These comparisons suggest that fishing bans were effective in reducing the number of detected boats in the Chinese EEZ around its outward boundary.

On the negative domain, i.e., just outside of the Chinese EEZ, boat density is significantly lower within 25 km of the EEZ border. The absence of a discontinuity in both periods implies that the decrease in boat density inside the Chinese EEZ during the ban periods is similar to the decrease in boat density just outside of the Chinese EEZ during the same periods. As one moves farther away from the border outward (leftward in Figure 6), the density gap between the ban-off and ban-on periods narrows.

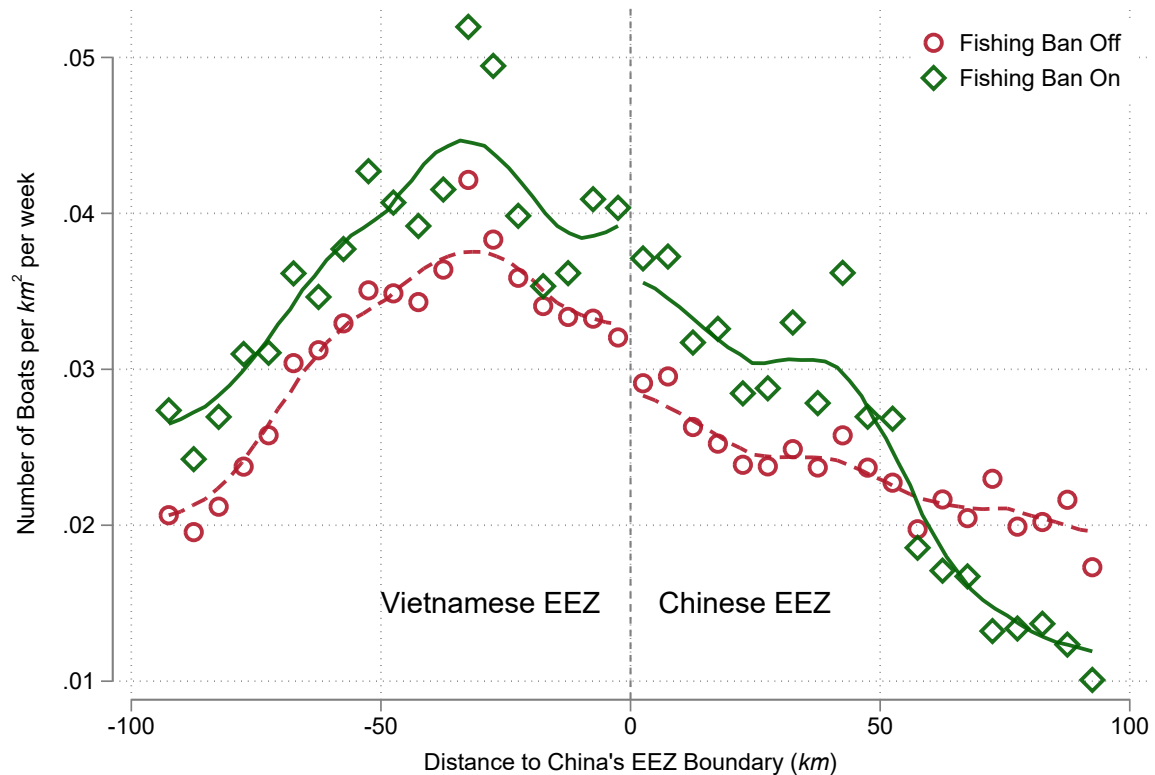
Given that the Chinese EEZ was more intensively fished during the ban-off periods compared to neighboring EEZs, the density gap between these periods just outside the Chinese EEZ suggests that Chinese fishermen may not have strictly adhered to fishing limits imposed by the EEZ boundary. The absence of a discontinuity at the EEZ border during both the fishing ban and non-ban periods also implies that fishing limits set by the EEZ border have not been consistently followed. It is unsurprising, considering the vast expanse of open ocean, the difficulties in patrolling, and the lack of advanced GPS systems on small fishing vessels to precisely determine and monitor their location relative to the EEZ border, that the EEZ border fails to create a spatial discontinuity in fishing activities.

Next, I present the spatial RD graph for the China-Vietnam EEZ border in Figure 7. Once again, circles indicate the ban-off period. Around the China-Vietnam EEZ border, the Vietnamese EEZ exhibited a higher boat density, which is in contrast to the other EEZ border segment. Moreover, at least within the Chinese EEZ and the Vietnamese EEZ close to the border, there is a downward gradient. This confirms that the Vietnamese side is more intensively fished than the Chinese side. Nevertheless, there is still no clear, discontinuous change in boat density at the border.

When we examine the hollow diamonds, representing boat density during the ban-on period, on the Vietnamese side (negative domain), the distance-density local polynomial fit is similar to that during the ban-off period, except at a higher level. It is interesting to note that the two boat density curves along the distance to the EEZ border on the Vietnamese side, i.e., the ban-off curve and ban-on curve, appear to parallel each other.

However, on the Chinese side (positive domain), within 50 km from the border, the boat density during the banned periods is higher than that during the no-ban periods. Beyond 50 km from the border, closer to the Chinese shore, the boat density during the banned periods falls below the boat density during the no-ban period.

Figure 7: Boat Density around the China-Vietnam EEZ Boundary



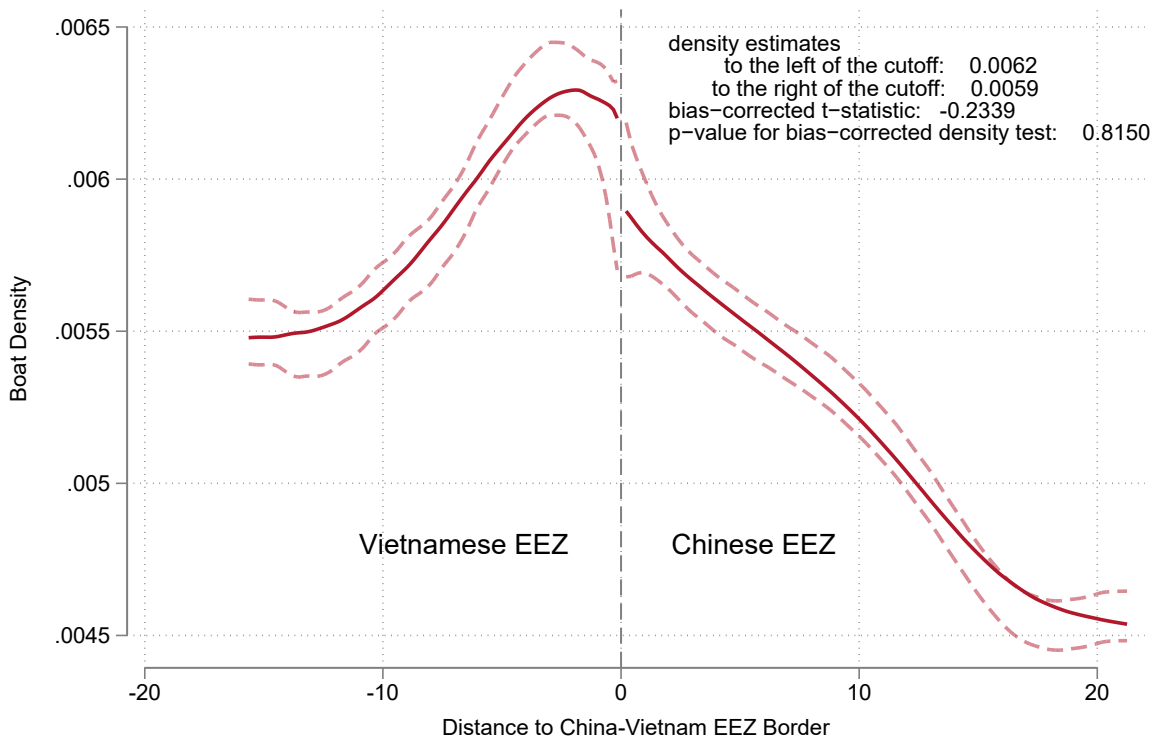
Notes: This figure shows the lack of boat density discontinuities at the China-Vietnam EEZ border during and outside fishing ban periods. Boat density is measured as detections per  $\text{km}^2$  per week, calculated from  $5 \text{ km} \times 5 \text{ km}$  grid cells. Red circles show average density during non-ban periods; green hollow diamonds show density during ban periods. Each point represents the average density within a  $5 \text{ km}$  distance bin from the border (marked by vertical dashed line at 0), extending to  $\pm 100 \text{ km}$ . Negative distances indicate Vietnamese waters; positive distances indicate Chinese waters. Sample includes all available boat detection data, aggregated separately for ban and non-ban periods. Densities are spatially averaged using grid cell centers for distance calculations.

To formally test the existence of a spatial discontinuity in boat density at the China-Vietnam EEZ border, I estimate the boat density on both sides of the border using a simple local polynomial density estimator proposed by [Cattaneo et al. \(2020\)](#). My focus is on the boat density during the fishing ban period. To simplify the problem from two dimensions to one dimension, I define the running variable as the distance between a location in the Gulf of Tonkin and the China-Vietnam EEZ border.

The simple local polynomial density estimator by [Cattaneo et al. \(2020\)](#) serves a similar objective to the density test by [McCrary \(2008\)](#). However, the [Cattaneo et al. \(2020\)](#) estimator does not require pre-binning of the data, eliminating the need to specify the bin width as an additional tuning parameter.

Figure 8 presents the local polynomial estimates of boat density during fishing ban periods around the China-Vietnam EEZ border, along with their 95% confidence intervals using the Jackknife method. As evident from the RD graph, there is no discernible discontinuity in boat density during the fishing ban at the China-Vietnam EEZ border. A bias-corrected test for the discontinuity in density yields a p-value of 0.815. Similarly, I did not find a statistically significant discontinuity in boat density for in whole outer border of Chinese EEZ.

Figure 8: Spatial Continuity of Boat Density around the China-Vietnam EEZ Boundary



Notes: This figure shows the local polynomial density estimates of boat distribution around the China-Vietnam EEZ border during fishing ban periods. The running variable is the distance to the border (km), with negative values indicating Vietnamese waters and positive values indicating Chinese waters. The solid red line shows the density estimate; dashed lines represent 95% confidence intervals using the Jackknife method with bias corrections. Density estimates are calculated using Cattaneo et al. (2020) simple local polynomial density estimator without pre-binning. Because bias correction is used for the construction of confidence intervals/bands, but not for point estimation, the confidence intervals may not be centered around the point estimates. The point estimates are constructed using local polynomial estimates of order 2, while the bias-corrected confidence intervals are constructed using local polynomial estimates of order 3. Point estimates of densities on either side of the cutoff are reported in the figure.

Collectively, Figure 6, Figure 7, and Figure 8 suggest that Chinese fishing vessels operate in neighboring countries' EEZs. Similarly, fishing vessels from neighboring countries may operate inside the Chinese EEZ.

The literature documents substantial spatial spillovers and inter-jurisdictional externalities in environmental policies (see, e.g., [Burgess et al., 2012](#); [Kahn et al., 2015](#); [Lipscomb and Mobarak, 2016](#)). Given that EEZ borders may not be strictly enforced, fishery regulations such as the Chinese fishing ban could generate significant spillover effects.

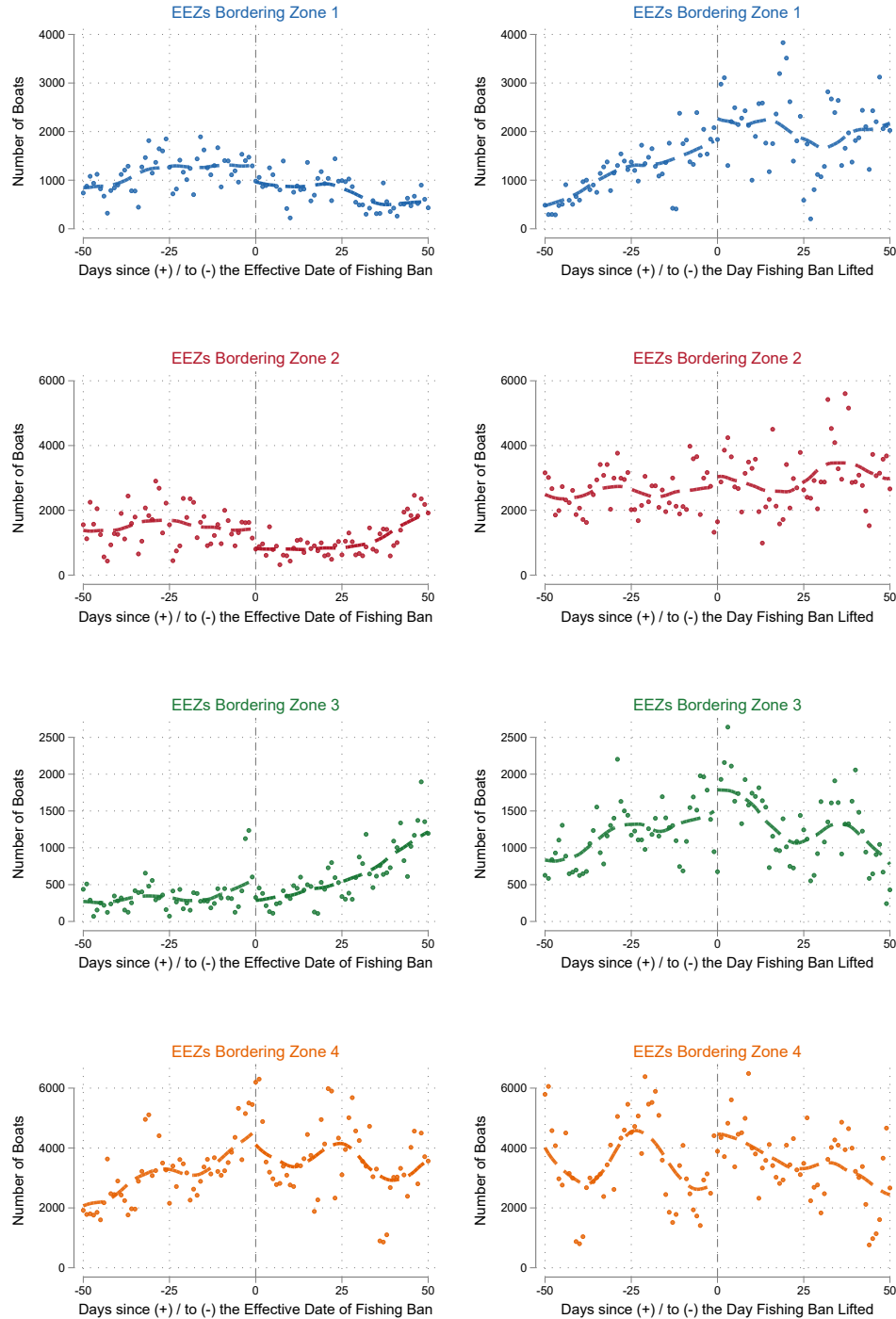
To investigate whether fishing bans in the Chinese EEZ affect vessel activity in neighboring EEZs, I apply the start and end dates of regulatory zones in Chinese waters to boat detection data in neighboring EEZs. In the absence of inter-jurisdictional spillovers, fishing bans in the Chinese EEZ should have no impact on boat detections in neighboring EEZs.

Figure 9 presents regression discontinuity plots analogous to the Chinese EEZ analysis in Figure 4, but focuses on boat detections in adjacent EEZs. For Zone 1, neighboring EEZs include North Korean and partial South Korean waters; for Zone 2, neighboring areas comprise parts of South Korean, Japanese, and Taiwanese EEZs; Zone 3 borders portions of Japanese and Taiwanese EEZs; and Zone 4 adjoins parts of Taiwanese and Vietnamese EEZs. Following VBD data conventions, analysis of waters neighboring the Chinese EEZ is restricted to areas west of 126.5 degrees East.

When fishing bans begin in Zones 1 through 3, boat detections in their respective neighboring EEZs show modest but significant decreases. The lifting of these bans produces less pronounced increases in boat detections in bordering EEZs, with the exception of Zone 4's neighboring waters.

Appendix Table A.3 reports nonparametric RD estimates following the structure of Table A.1. While statistically significant decreases in boat detections occur in only three zones' neighboring waters when bans begin, point estimates are negative across all four zones at ban initiation and positive when bans are lifted. These results provide evidence that the Chinese fishing ban generates substantial spillover effects on vessel activity in neighboring EEZs.

Figure 9: RDiT of Boat Detections in Neighboring EEZs



Notes: This figure shows regression discontinuity plots examining boat detections in EEZs neighboring Chinese regulatory zones around China's fishing ban transitions. Each row represents a different Chinese regulatory zone and its neighboring EEZs: Zone 1 (North Korea, South Korea), Zone 2 (South Korea, Japan, Taiwan), Zone 3 (Japan, Taiwan), and Zone 4 (Taiwan, Vietnam). Left panels show changes when Chinese bans begin; right panels show changes when bans end. Each dot represents the total number of boats detected in neighboring EEZs, aggregated by nights before/after ban transitions. Day 0 marks the first night following the transition. The x-axis spans 50 nights before and after transitions. Solid lines show local polynomial fits. Sample covers 2012-2017, with neighboring waters defined as EEZs sharing boundaries with Chinese regulatory zones west of 126.5°E.

## 7 Fishing Efforts & Discussions

### 7.1 Fishing Efforts

One major limitation of boat detection from remote sensing images is that we do not know the origin of the boat. There are several reasons to have the spillover identified in the last section. For example, Chinese fishing vessels may have fished in Vietnamese EEZ outside of the ban period. When fishing ban applies to Chinese EEZ, not being able to fish in Chinese EEZ may reduce the profitability of fishing at all, which lowers the boat detection in Vietnamese EEZs. Alternatively, to the extent that the enforcement of fishing ban relies on complementary measure of onshore inspection, Chinese vessels may not be able to sail to Vietnamese EEZ to operate. If so, the reduction in boat detected in Vietnamese during the Chinese fishing bans are mainly due to the absence of Chinese vessels.

On the other hand, if the absence of rival fishing vessels and limited patrolling capacity in Chinese EEZ attract Vietnamese fishing vessels to fish in Chinese EEZ during the fishing ban, then Chinese fishing bans crowd in Vietnamese fishing in their EEZs. A larger share of boat detected in Chinese EEZ may be from Vietnamese. And the crowd-in presents an example of regulatory free-riding.

To investigate the nature of spillover, I analyze the AIS-based dataset on fishing effort from Global Fishing Watch. Because AIS signals include a vessel's identity, in particular, the registered country, it may be potentially informative on the nature of EEZ incursions. In the AIS-based dataset, fishing vessels may be uniquely identified by their MMSI (Maritime Mobile Service Identity), which is a unique nine-digit number used to identify vessels in maritime communications.

Independently, fishing effort is of interest as its more directly related marine catch and therefore policy questions on sustainable fishery. If, for example, the number of boats operating during fishing ban decrease but on average each vessels fish more intensively, then the fishing ban may not achieve its policy goals for environmental sustainability.

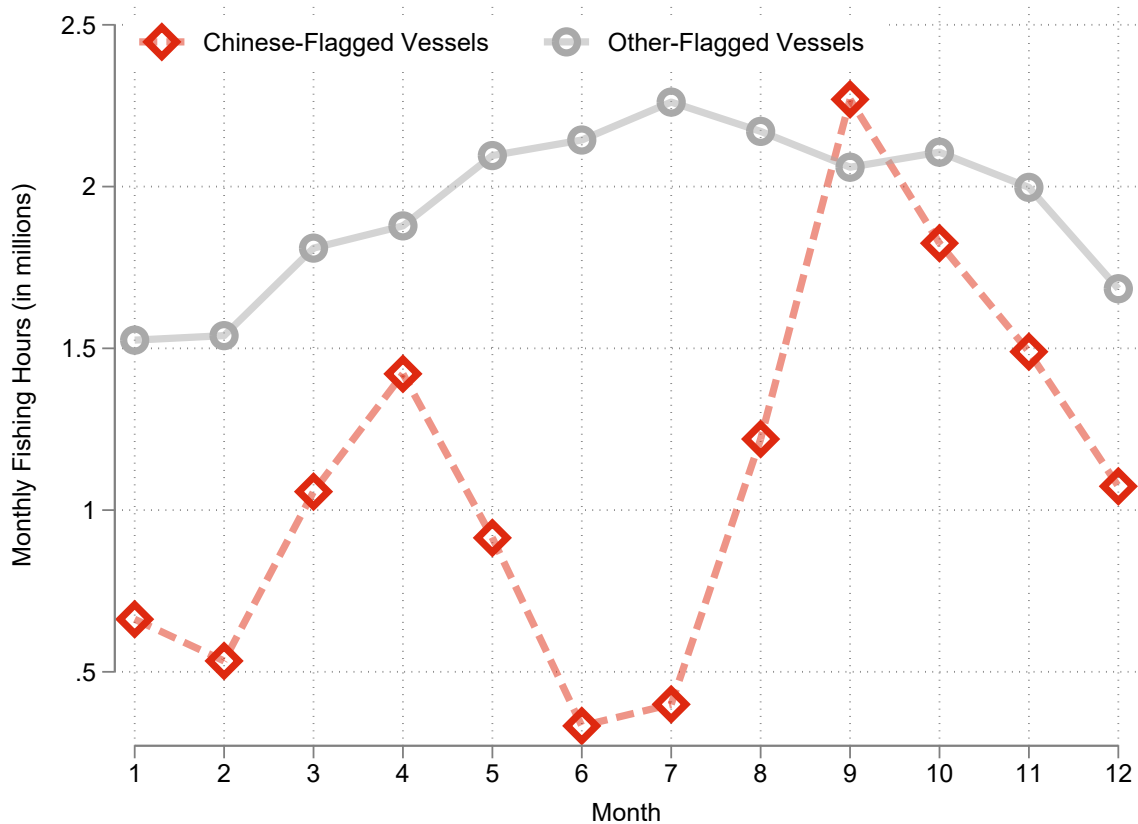
The drawback of AIS-based measure for fishing activities is that they only capture vessels that install AIS devices, which tend to be larger vessels. To illustrate, in the dataset, there were 73,938 vessels that registered in China and operated in 2015. Less than 1% of these vessels had a length less than 12 meters. However, as shown in Table 1, close to 68.6% of seafaring fishing vessels were less than 12 meter.

On the other hand, fishing vessels with at least 12 meter long account for 90% of tonnage of fishing vessels in China ([China Fishery Statistical Year Book, 2016](#)). A significant portion of larger vessels are equipped with AIS. Larger vessels are more powerful and have more capacity for fishing operation. Therefore, a considerable portion of the global fish catch likely comes from vessels with AIS. Moreover, the fishing vessels recorded in the fishing effort data set represent about 86% of registered fishing vessels with at least 12 meter long in China in 2014.

Figure 10 shows the global fishing effort by month, as measured by the total monthly fishing hours per month. The GFW fishing effort cover years 2012 to 2020. Figure 10 represents the average over these years. The red diamond symbol and dashed line represent all fishing vessels registered in China. The hollow circle and solid line in gray represent vessels registered in other countries.

There is a strong seasonality, even outside of ban period, in fishing efforts among Chinese vessels, and to a less extent among non-Chinese vessels. Fishing efforts by Chinese vessels account for a considerable portion of global fishing effort. During fishing ban, fishing effort by Chinese vessels drop sharply, reaching bottom in June, when was the first full month when all Chinese EEZ was under fishing ban between 2012 and 2016. Chinese vessels' fishing effort rebounds strongly as fishing bans are lifted. Indeed, September sees the highest fishing effort from Chinese fishing vessels, more than the combined fishing efforts from vessels from the rest of the world.

Figure 10: Global Fishing Efforts by Month



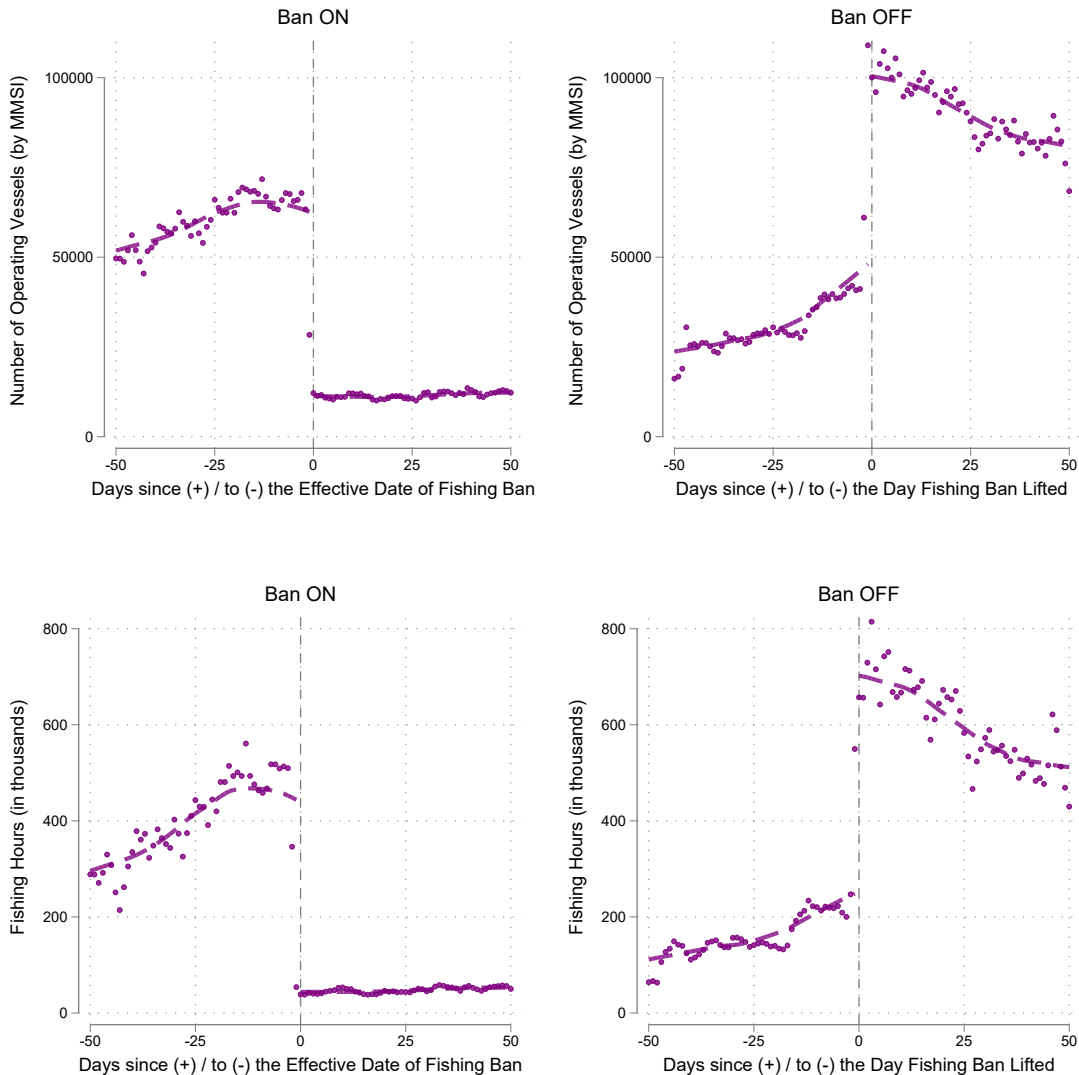
Notes: This figure shows average monthly global fishing effort from 2012-2020, measured in millions of fishing hours, based on Global Fishing Watch AIS data. Red diamonds and dashed line represent Chinese-flagged vessels; gray circles and solid line represent vessels flagged to all other countries. Fishing effort is detected and classified using Global Fishing Watch's neural network algorithm applied to AIS transmissions from fishing vessels. Monthly values represent the sum of fishing hours across all vessels within each flag category. The figure averages across all years in the sample period.

To assess how the fishing ban affects the fishing effort in Chinese EEZ, I match the 0.1 degree cells from the GFW data on fishing effort to regulatory zones of Chinese EEZ. I focus on two measures of fishing activities. The first one is the number of fishing vessels presented in Chinese EEZ. Although the subset of vessels observed in the GFW AIS-based data tend to be larger, the number of vessels active in Chinese EEZ provide a direct comparison to the boat detections from the satellite date. The RD plots on the top row in Figure 11 represent this measure of fishing activities on their y-axis.

The second measure is the total number of hours operating in Chinese EEZ. For the observed set of vessels, this measure most directly related to fishing intensity in a particular area. To the extent that vessels with AIS account for a substantial portion of fishing activities in the Chinese EEZ, this measure informs on the fishing intensity in the Chinese EEZ at a high temporal frequency, namely daily. The RD plots on the bottom row in Figure 11 represent this measure of fishing activities on their y-axis.

As in previous RD figures, the plots on the left in Figure 11 center on the start of fishing bans, while the plots on the right center on the end of fishing bans. As in Figure 3, I aggregate the fishing activities across the 4 regulatory zone across years by the temporal distance to the transition of fishing bans (in days).

Figure 11: Fishing Effort based on AIS Signals around the Starts and Ends of Fishing Bans



Notes: This figure shows regression discontinuity plots examining two measures of fishing activity around China's fishing ban transitions. The top panels show the number of unique fishing vessels (by MMSI) detected in Chinese EEZ; the bottom panels show total fishing hours (in thousands). Left panels examine changes when bans begin ("Ban ON"); right panels show changes when bans end ("Ban OFF"). Each point represents daily aggregated activity across all regulatory zones, averaged across years 2012-2020. Day 0 marks the transition date, with the x-axis showing 50 days before and after transitions. Data are from Global Fishing Watch's AIS-based fishing effort dataset, aggregated from 0.1-degree grid cells matched to Chinese regulatory zones. Dashed lines show local polynomial fits on each side of the cutoff.

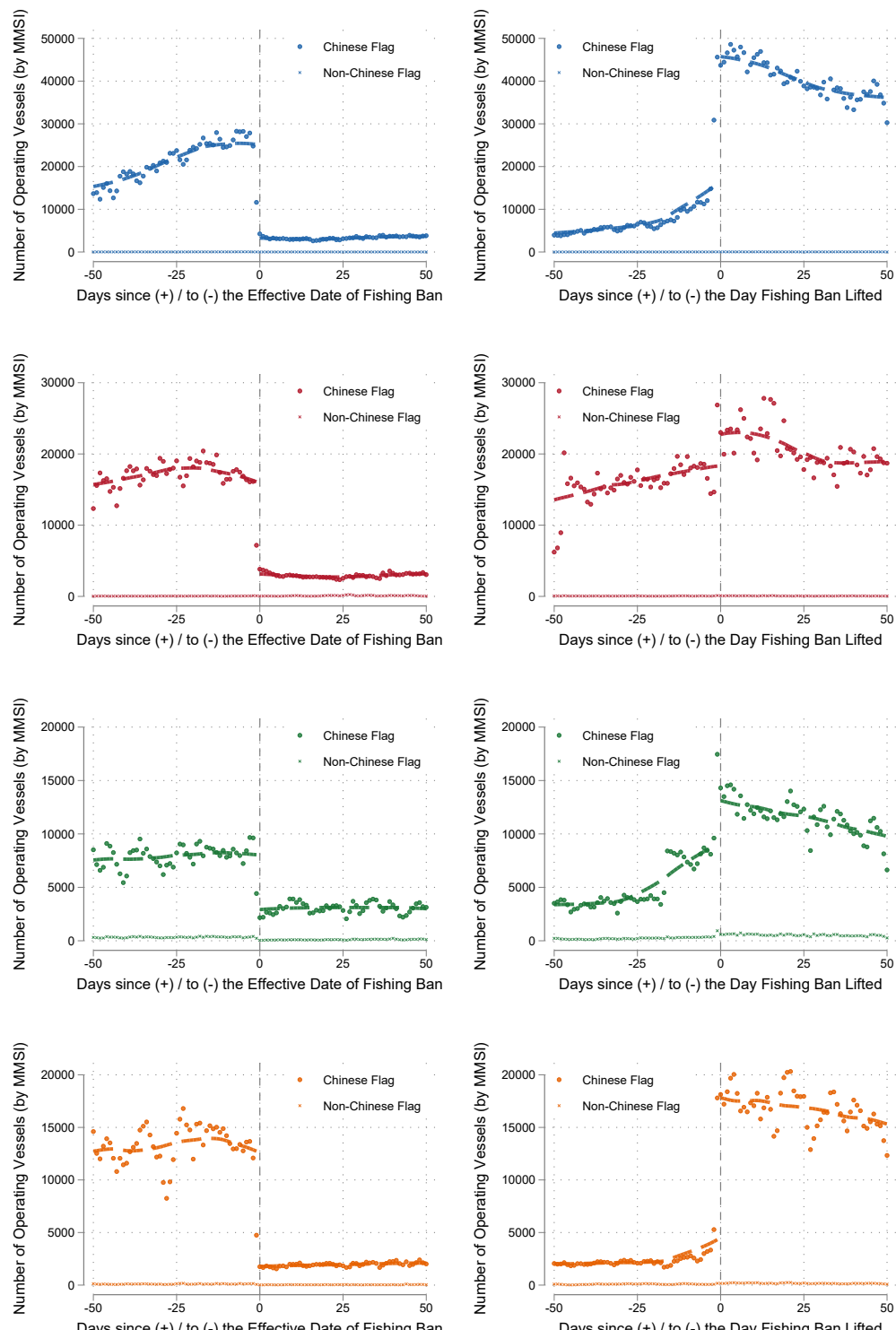
Figure 11 shows similar patterns as the RD plots in Figure 3. If anything, the discontinuities around the ban starts and ends are sharper. Perhaps unlike satellite based measures, AIS-based measurement is much less affected by weather conditions such as cloud coverage. But it is also possible that because their larger size, and their emission of AIS-signals, the enforcement of fishing bans against, and therefore their compliance, may be high. Interestingly, in the AIS-based data, we also see that on the day before ban starts, there has been already a drop in the present and fishing efforts of fishing vessels.

Notice that Figure 11 plots the fishing activities in Chinese EEZ regardless the flag states of the vessels. To see whether foreign vessels operate in Chinese EEZ and how the fishing ban affects fishing activities in each regulatory zone, Figure 12 includes 8 RD plots in a structure similar to that of Figure 4 except that the outcome variable is the total fishing hours in the zone instead of boat detections.

The number of vessels by foreign flags in each plot is close to the horizontal axis and barely visual. This is because, during fishing ban or not, the more than 99% of fishing vessels with AIS signals that operated in Chinese EEZ were Chinese vessels. Outside the fishing bans, 0.9% of fishing vessels operating in Chinese EEZ carry foreign flags. During fishing bans, however, their share increases to 1.6%.

If we focused on the counts of Chinese vessels, the patterns in Figure 13 again echos those we observe from RD graphics on the boat detections. One difference is, however, that the drop of vessels count at the start of fishing ban now is very similar to the increase of vessels count at the end of fishing bans.

Figure 12: Vessel Counts based on AIS Signals around the Starts and Ends of Fishing Bans: by Zone & by Vessel Flag



Notes: This figure shows RD plots examining the number of operating fishing vessels (identified by MMSI) separately for Chinese and non-Chinese flagged vessels in each regulatory zone. Each row represents a different zone (Zones 1-4 from top to bottom). Left panels show changes when bans begin; right panels show changes when bans end. Blue/red/green/orange dots represent Chinese-flagged vessels; gray dots represent non-Chinese flagged vessels. Each point represents the daily count of unique vessels operating in the zone, aggregated across years 2012-2020. Day 0 marks the transition date, with the x-axis showing 50 days before and after transitions. Dashed lines show local polynomial fits.

If we turn to fishing hours in Figure 13 instead of vessel count, a similar pattern emerges. Both vessel count and fishing hours were consistently low during fishing bans. In unreported Donut Hole RDiT estimates, the rises and drops in fishing hours at the lifting and start of bans tend to be larger than the corresponding changes in vessel counts. In the AIS-based data, larger, heavier, and more powerful vessels average more fishing hours per year. This is expected, as larger vessels likely have greater storage and refrigeration capacity, can travel farther, and have more crew members to specialize in different parts of the fishing operation. If this correlation extends to smaller vessels without AIS devices, then the detection count may underestimate the effect of fishing bans on fishing effort. On the other hand, although there has been some uptake of AIS-equipped vessels in Zones 1 and 3, it is likely that there are more ban violations by smaller vessels, whether Chinese-flagged or otherwise.

Although Chinese vessels dominate fishing activity in the Chinese EEZ, the presence of foreign vessels nearly doubled from 0.9% to 1.6% during ban periods. The change in fishing effort is even more pronounced: foreign vessels account for 0.7% of fishing hours in the Chinese EEZ during non-ban periods but approximately 2% during ban periods. Vietnamese vessels provide a striking example of this pattern. While they account for only 0.02% of fishing hours in Chinese EEZ during non-ban periods, their share increases to 0.33% during ban periods. Notably, this increase is not merely an artifact of reduced Chinese fishing activity in the denominator. The absolute number of fishing hours by Vietnamese vessels during the three-month ban period exceeds their total fishing hours during the approximately nine months outside the ban period.

The spillover evidence presented in Figure 9 suggests that Chinese vessels also operate in neighboring EEZs. Outside of the fishing ban in Zone 4, Chinese vessels make up 39.4% of AIS-enabled vessels and 41.5% of fishing hours in the Vietnamese EEZ. During the fishing ban, however, the share of Chinese vessels in the Vietnamese EEZ drops to 15%, and their share of fishing hours decreases to 14.4%.

The presence of EEZ incursions by both foreign and Chinese vessels suggests that offshore patrolling and deterrence alone are insufficient to enforce fishing bans effectively. Complementary onshore measures, such as port inspections or the lock-up of fishing gear, are essential to support enforcement. Given the decentralized fishery management structure in China, the international spillover of fishery regulations also points to the potential for spillovers across regulatory zones within the country.

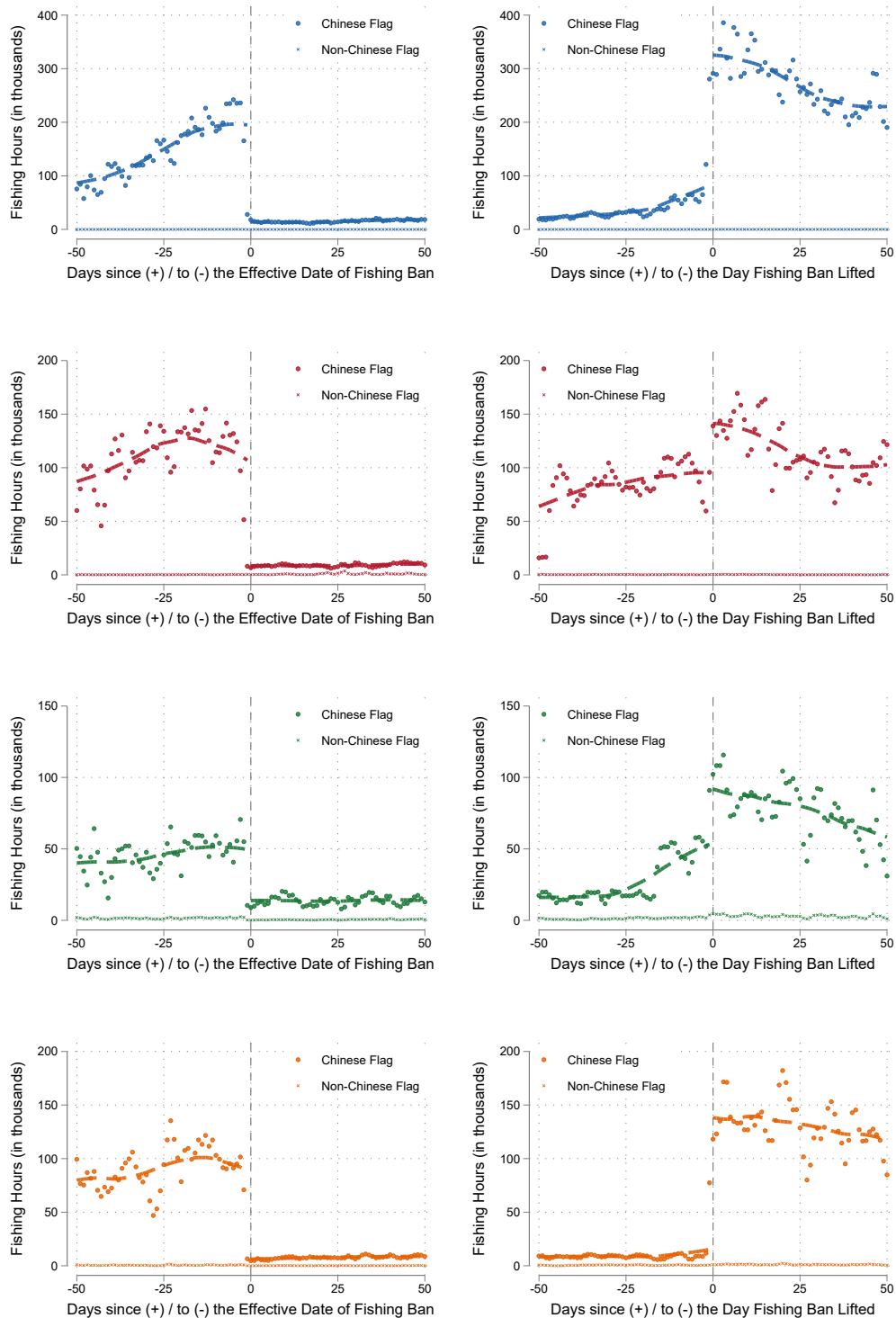
Zones 3 and 4 have historically ended their bans earlier than Zones 1 and 2 and also started their bans earlier prior to 2017. Figure A.5 in the Appendix explores this inter-

jurisdictional spillover within China. The RD plots on the left apply the earlier start dates in Zones 3 and 4 to boat detections in Zones 1 and 2 between 2012 and 2016, while the RD plots on the right apply the earlier end dates in Zones 3 and 4 to boat detections in Zones 1 and 2 between 2012 and 2017. There is some evidence that the start of fishing bans in Zones 3 and 4 reduces boat detections in Zones 1 and 2, though the RD estimates are not statistically significant at conventional levels. However, the end of fishing bans in Zones 3 and 4 is associated with increased boat detections in Zones 1 and 2. The nonparametric estimates for Zones 1 and 2 are statistically significant at the 1% and 10% levels, respectively. The point estimate for Zone 2, which is adjacent to Zone 3, is considerably larger than that for Zone 1.

It is important to note one confounding factor that cautions against a causal interpretation of these findings. Starting on August 1st, certain fishing methods were exempted in Zones 1 and 2, coinciding with the end of fishing bans in Zones 3 and 4 before 2017.

Nevertheless, the potential spillovers across regulatory zones and the challenges they pose to enforcing fishing bans were serious enough for Beijing to align the starting dates of fishing bans across all four zones in 2017.

Figure 13: Fishing Hours based on AIS Signals around the Starts and Ends of Fishing Bans: by Zone & by Vessel Flag



Notes: This figure shows RD plots examining the apparent fishing hours in each regulatory zone. Each row represents a different zone (Zones 1-4 from top to bottom). Left panels show changes when bans begin; right panels show changes when bans end. Blue/red/green/orange dots represent Chinese-flagged vessels; gray dots represent non-Chinese flagged vessels. Each point represents the daily fishing hours in the zone, aggregated across years 2012-2020. Day 0 marks the transition date, with the x-axis showing 50 days before and after transitions. Dashed lines show local polynomial fits.

## 7.2 AIS Disabling Events

As mentioned in Section 3.5, a limitation of AIS data is that AIS devices can be turned off to evade monitoring, particularly during potentially illegal fishing activities. To assess the prevalence of AIS disabling within and near China's EEZ, I examine the [Welch et al. \(2022\)](#) dataset on AIS-disabling events from Global Fishing Watch. Specifically, I focus on AIS-disabling events involving Chinese-flagged vessels, which are mapped in Appendix Figures A.6. Notably, most AIS-disabling events by Chinese-flagged vessels occur far from China's EEZ, with many taking place in international waters just outside the Japanese and Peruvian EEZs. Likewise, I find few AIS-disabling events near or within China's EEZ by non-Chinese-flagged vessels.

In theory, fishing vessels could evade detection by turning off their lights, potentially causing our satellite-based remote sensing data to underestimate the extent of illegal fishing. In such cases, nighttime boat detection data would overstate the fishing bans' effectiveness for fishery management. However, several factors may limit such avoidance behavior. First, VIIRS can detect low light emissions, although detection capability depends on cloud cover and weather conditions. If some minimum lighting is necessary for safe marine operations, vessels may still be captured in satellite images. Second, while China has exclusive rights to marine resources within its EEZ, it cannot prohibit maritime navigation. To enforce fishing regulations, authorities must board suspected vessels to inspect catches. Spotting a vessel at a distance may be insufficient for enforcement, as vessels can evade inspection. Finally, the substantial continued fishing activity by AIS-equipped vessels, which are larger and easily identifiable at a distance, suggests that the risk of inspection by offshore patrol authorities may be limited. Nevertheless, since we cannot quantify the prevalence of light-based avoidance strategies, this limitation warrants consideration when interpreting our results.

## 8 Concluding Remarks

This paper examines the effectiveness of China's seasonal fishing bans in curbing fishing activities within its Exclusive Economic Zone (EEZ). The findings indicate that the bans, though not perfectly enforced, lead to significant reductions in both boat detections and fishing hours during the ban periods. This impact highlights the potential of command-and-control policies for resource management in contexts where market-based mechanisms may be challenging to implement.

Several complementary factors likely enhance the effectiveness of these bans, including coordinated offshore patrols, inspections, and the availability of aquaculture alternatives that mitigate consumer demand during the ban period. However, some evidence suggests that enforcement effectiveness declines over time, with fishing activities gradually resuming toward the later stages of the bans.

The study also underscores the importance of considering inter-jurisdictional spillovers. Chinese vessels operating in neighboring EEZs during ban periods and foreign vessels increasing their activities in the Chinese EEZ suggest that cooperation with adjacent nations could enhance policy efficacy.

Overall, this analysis contributes to understanding the conditions under which seasonal fishing bans can achieve sustainable fishery objectives. Further research could examine heterogeneity in ban compliance across different vessel types and explore additional regulatory tools to complement seasonal bans.

## References

- Anderson, Michael L (2014) "Subways, Strikes, and Slowdowns: the Impacts of Public Transit on Traffic Congestion," *American Economic Review*, 104 (9), 2763–96.
- Assunção, Juliano, Clarissa Gandour, and Romero Rocha (2023) "DETER-ing Deforestation in the Amazon: Environmental Monitoring and Law Enforcement," *American Economic Journal: Applied Economics*, 15 (2), 125–56.
- Auffhammer, Maximilian and Ryan Kellogg (2011) "Clearing the Air? The Effects of Gasoline Content Regulation on Air Quality," *American Economic Review*, 101 (6), 2687–2722.
- Axbard, Sebastian (2016) "Income Opportunities and Sea Piracy in Indonesia: Evidence from Satellite Data," *American Economic Journal: Applied Economics*, 8 (2), 154–94.
- Barreca, Alan I., Melanie Guldin, Jason M. Lindo, and Glen R. Waddell (2011) "Saving Babies? Revisiting the Effect of Very Low Birth Weight Classification," *Quarterly Journal of Economics*, 126, 2117–2123.
- Besley, Timothy, Thiemo Fetzer, and Hannes Mueller (2015) "The Welfare Cost of Lawlessness: Evidence from Somali Piracy," *Journal of the European Economic Association*, 13 (2), 203–239.
- Bos, Björn (2021) "Fishing under the Radar: Estimating Compliance with Fishing Bans," September, 10.2139/ssrn.3871993, Available at SSRN: <https://ssrn.com/abstract=3871993>.
- Brown, Gardner M (2000) "Renewable Natural Resource Management and Use Without Markets," *Journal of Economic Literature*, 38 (4), 875–914.
- Burgess, Robin, Matthew Hansen, Benjamin A. Olken, Peter Potapov, and Stefanie Sieber (2012) "The Political Economy of Deforestation in the Tropics," *Quarterly Journal of Economics*, 127 (4), 1707–1754, 10.1093/qje/qjs034.
- Calonico, Sebastian, Matias D Cattaneo, and Rocio Titiunik (2014) "Robust Nonparametric Confidence Intervals for Regression-Discontinuity Designs," *Econometrica*, 82 (6), 2295–2326.
- Carruthers, Bruce G and Naomi R Lamoreaux (2016) "Regulatory races: the effects of jurisdictional competition on regulatory standards," *Journal of Economic Literature*, 54 (1), 52–97.
- Cattaneo, Matias D, Michael Jansson, and Xinwei Ma (2020) "Simple Local Polynomial Density Estimators," *Journal of the American Statistical Association*, 115 (531), 1449–1455.

- Chan, H Ron and Christy Zhou (2023) "Charged Up? Distributional Impacts of Green Energy on Local Labor Markets," *SSRN Working Paper*, [https://papers.ssrn.com/sol3/papers.cfm?abstract\\_id=4534479](https://papers.ssrn.com/sol3/papers.cfm?abstract_id=4534479).
- Chan, H Ron and Yichen Christy Zhou (2021) "Regulatory Spillover and Climate Co-benefits: Evidence From New Source Review Lawsuits," *Journal of Environmental Economics and Management*, 110, 102545.
- Chang, Ni-Na, Jen-Chieh Shiao, and Gwo-Ching Gong (2012) "Diversity of Demersal Fish in the East China Sea: Implication of Eutrophication and Fishery," *Continental Shelf Research*, 47, 42–54, 10.1016/j.csr.2012.whatever.
- Chen, Yihsu and Alexander Whalley (2012) "Green Infrastructure: The Effects of Urban Rail Transit on Air Quality," *American Economic Journal: Economic Policy*, 4 (1), 58–97.
- China Fishery Statistical Year Book (2016) *China Fishery Statistical Year Book*: China Agriculture Press.
- Conley, Timothy G (1999) "GMM Estimation with Cross Sectional Dependence," *Journal of Econometrics*, 92 (1), 1–45.
- Cropper, Maureen L and Wallace E Oates (1992) "Environmental Economics: A Survey," *Journal of Economic Literature*, 30 (2), 675–740.
- Davis, Lucas W. (2008) "The Effect of Driving Restrictions on Air Quality in Mexico City," *Journal of Political Economy*, 116 (1), 38–81.
- Donaldson, Dave and Adam Storeygard (2016) "The View from Above: Applications of Satellite Data in Economics," *Journal of Economic Perspectives*, 30 (4), 171–98.
- Elvidge, Christopher D, Kimberly E Baugh, Mikhail Zhizhin, and Feng-Chi Hsu (2013) "Why VIIRS Data Are Superior to Dmsp for Mapping Nighttime Lights," *Proceedings of the Asia-Pacific Advanced Network*, 35, 62–69.
- Elvidge, Christopher D, Kimberly Baugh, Mikhail Zhizhin, Feng Chi Hsu, and Tilotama Ghosh (2017) "VIIRS Night-time Lights," *International Journal of Remote Sensing*, 38 (21), 5860–5879, 10.1080/01431161.2017.1342050.
- Elvidge, Christopher D, Mikhail Zhizhin, Kimberly Baugh, and Feng-Chi Hsu (2015a) "Automatic Boat Identification System for VIIRS Low Light Imaging Data," *Remote Sensing*, 7 (3), 3020–3036.
- Elvidge, Christopher D, Mikhail Zhizhin, Kimberly Baugh, Feng-Chi Hsu, and Tilotama Ghosh (2015b) "Methods for Global Survey of Natural Gas Flaring from Visible Infrared Imaging Radiometer Suite Data," *Energies*, 9 (1), 14.
- FAO (2002) "Fishery Statistics: Reliability and Policy Implications," *memorandum*.

FAS Staff (2021) "2021 China's Fishery Report," Voluntary Report CH2021-0176, United States Department of Agriculture Foreign Agricultural Service, Beijing, Public Distribution Date: December 22, 2021.

Fisher, Ronald A. (1935) *The Design of Experiments*, Edinburgh: Oliver and Boyd, 1st edition.

Flückiger, Matthias and Markus Ludwig (2015) "Economic Shocks in the Fisheries Sector and Maritime Piracy," *Journal of Development Economics*, 114, 107–125.

Hausman, Catherine and David S Rapson (2018) "Regression Discontinuity in Time: Considerations for Empirical Applications," *Annual Review of Resource Economics*, 10, 533–552.

He, Guojun, Shaoda Wang, and Bing Zhang (2020) "Watering Down Environmental Regulation in China," *Quarterly Journal of Economics*, 135 (4), 2135–2185.

Henderson, J. Vernon, Adam Storeygard, and David N. Weil (2012) "Measuring Economic Growth from Outer Space," *American Economic Review*, 102 (2), 994–1028, 10.1257/aer.102.2.994.

Hodler, Roland and Paul A. Raschky (2014) "Regional Favoritism," *Quarterly Journal of Economics*, 129 (2), 995–1033, 10.1093/qje/qju004.

Hu, Chuanmin, Lian Feng, Zhongping Lee, Bryan A Franz, Sean W Bailey, P Jeremy Werdell, and Christopher W Proctor (2019) "Improving satellite global chlorophyll a data products through algorithm refinement and data recovery," *Journal of Geophysical Research: Oceans*, 124 (3), 1524–1543.

Kahn, Matthew E, Pei Li, and Daxuan Zhao (2015) "Water Pollution Progress at Borders: the Role of Changes in China's Political Promotion Incentives," *American Economic Journal: Economic Policy*, 7 (4), 223–42.

Kroodsma, David A, Juan Mayorga, Timothy Hochberg et al. (2018) "Tracking the global footprint of fisheries," *Science*, 359 (6378), 904–908.

Lipscomb, Molly and Ahmed Mushfiq Mobarak (2016) "Decentralization and Pollution Spillovers: Evidence from the Re-Drawing of County Borders in Brazil," *Review of Economic Studies*, 84 (1), 464–502.

McCrary, Justin (2008) "Manipulation of the Running Variable in the Regression Discontinuity Design: A Density Test," *Journal of Econometrics*, 142 (2), 698–714.

Michalopoulos, Stelios and Elias Papaioannou (2013) "National Institutions and Sub-national Development in Africa," *Quarterly Journal of Economics*, 129 (1), 151–213.

Ministry of Agriculture (2017) "Most Restrictive Fishing Conservation Policy Protects Marine Fishery Resources," *Press Office of the Chinese Ministry of Agriculture*, [http://jiuban.moa.gov.cn/zwllm/zwdt/201708/t20170803\\_5768337.htm](http://jiuban.moa.gov.cn/zwllm/zwdt/201708/t20170803_5768337.htm).

Ministry of Agriculture and Rural Affairs of the People's Republic of China (2019) 2019 [China Fishery Statistical Yearbook 2019], Beijing: China Agriculture Press.

Newey, Whitney K. and Kenneth D. West (1986) "A Simple, Positive Semi-definite, Heteroskedasticity and Autocorrelation Consistent Covariance Matrix," *Econometrica*, 55 (3), 703–08.

Semedi, Bambang and A Luthfi Hadiyanto (2013) "Forecasting the fishing ground of small pelagic fishes in Makassar Strait using moderate resolution Image Spectroradiometer Satellite Images," *Journal of Applied Environmental and Biological Sciences*, 3 (2), 29–34.

Sigman, Hilary (2002) "International Spillovers and Water Quality in Rivers: Do Countries Free Ride?" *American Economic Review*, 92 (4), 1152–1159.

Tibshirani, Robert (1996) "Regression Shrinkage and Selection via the Lasso," *Journal of the Royal Statistical Society: Series B (Methodological)*, 58 (1), 267–288, 10.1111/j.2517-6161.1996.tb02080.x.

U.N. Food and Agriculture Organization (2014) "The State of World Fisheries and Aquaculture," *FAO Fisheries and Aquaculture Department*.

——— (2016) "The State of World Fisheries and Aquaculture," *FAO Fisheries and Aquaculture Department*.

Walker, W Reed (2011) "Environmental regulation and labor reallocation: Evidence from the Clean Air Act," *American Economic Review*, 101 (3), 442–447.

Watson, Reg and Daniel Pauly (2001) "Systematic Distortions in World Fisheries Catch Trends," *Nature*, 414 (6863), 534.

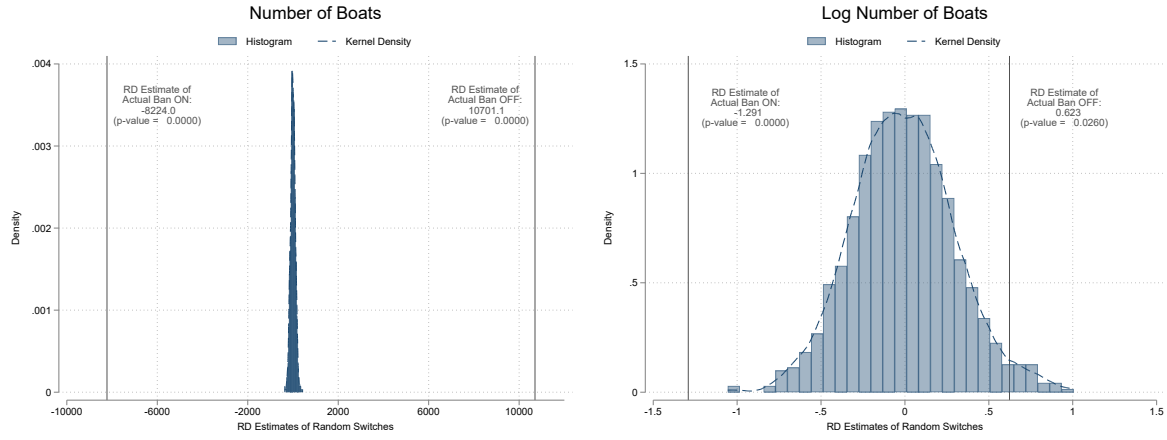
Welch, Heather, Tyler Clavelle, Timothy D. White, Megan A. Cimino, Jennifer Van Osdel, Timothy Hochberg, David Kroodsma, and Elliott L. Hazen (2022) "Hot Spots of Unseen Fishing Vessels," *Science Advances*, 8 (44), eabq2109, 10.1126/sciadv.abq2109.

Yan, Zhaojin, Rong He, Xiaoguang Ruan, and Hui Yang (2022) "Footprints of Fishing Vessels in Chinese Waters Based on Automatic Identification System Data," *Journal of Sea Research*, 187, 102255, 10.1016/j.seares.2022.102255.

Yu, Yi, Xiaogang Xing, Hailong Liu, Yeping Yuan, Yuntao Wang, and Fei Chai (2019) "The variability of chlorophyll-a and its relationship with dynamic factors in the basin of the South China Sea," *Journal of Marine Systems*, 200, 103230, 10.1016/j.jmarsys.2019.103230.

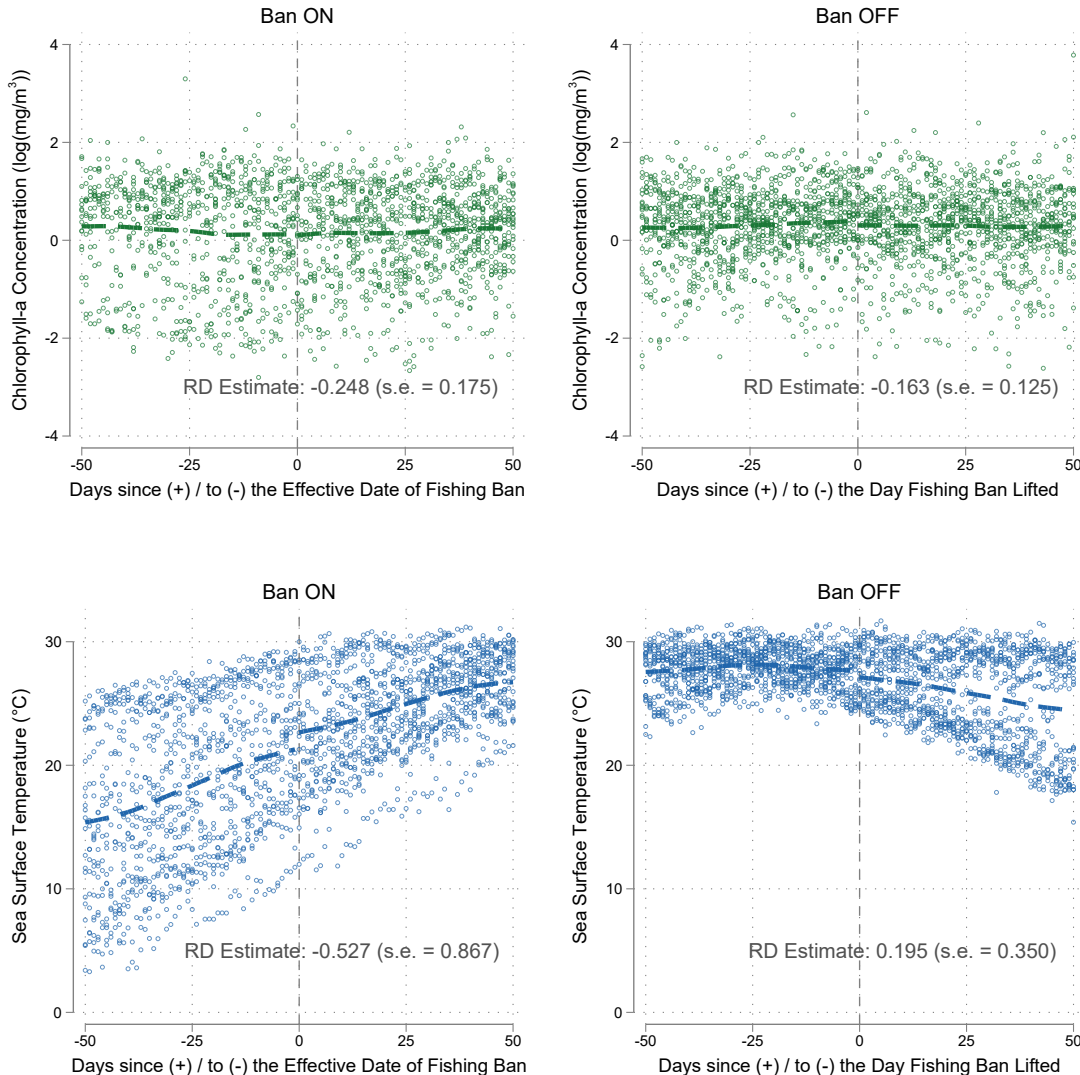
# **Appendix**

Figure A.1: Randomization Inference



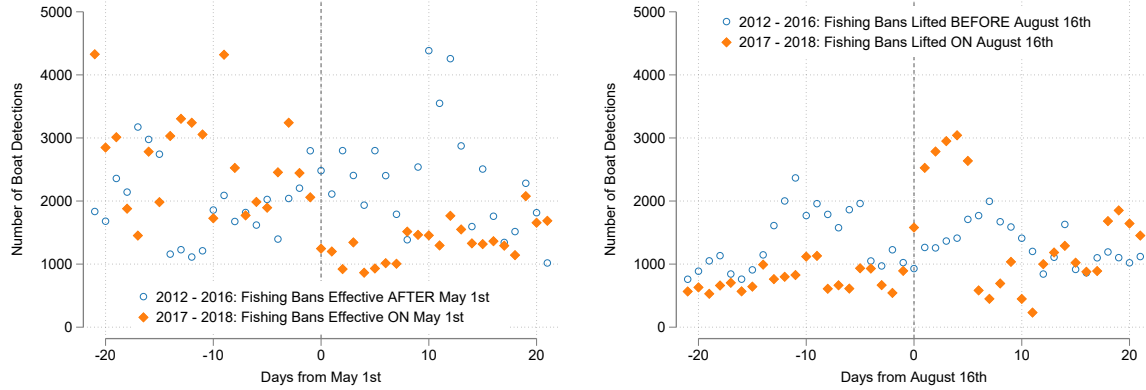
Notes: This figure presents the distribution of placebo estimates from 1,000 simulations that randomize fishing ban start and end dates across regulatory zones and years. The left histogram shows estimates using the number of boat detections as the dependent variable; the right histogram uses the log number of boat detections. Vertical lines indicate the actual nonparametric RD estimates for ban start and end dates, with corresponding randomization inference p-values.

Figure A.2: Continuity Tests and Plots with Oceanographic Variables



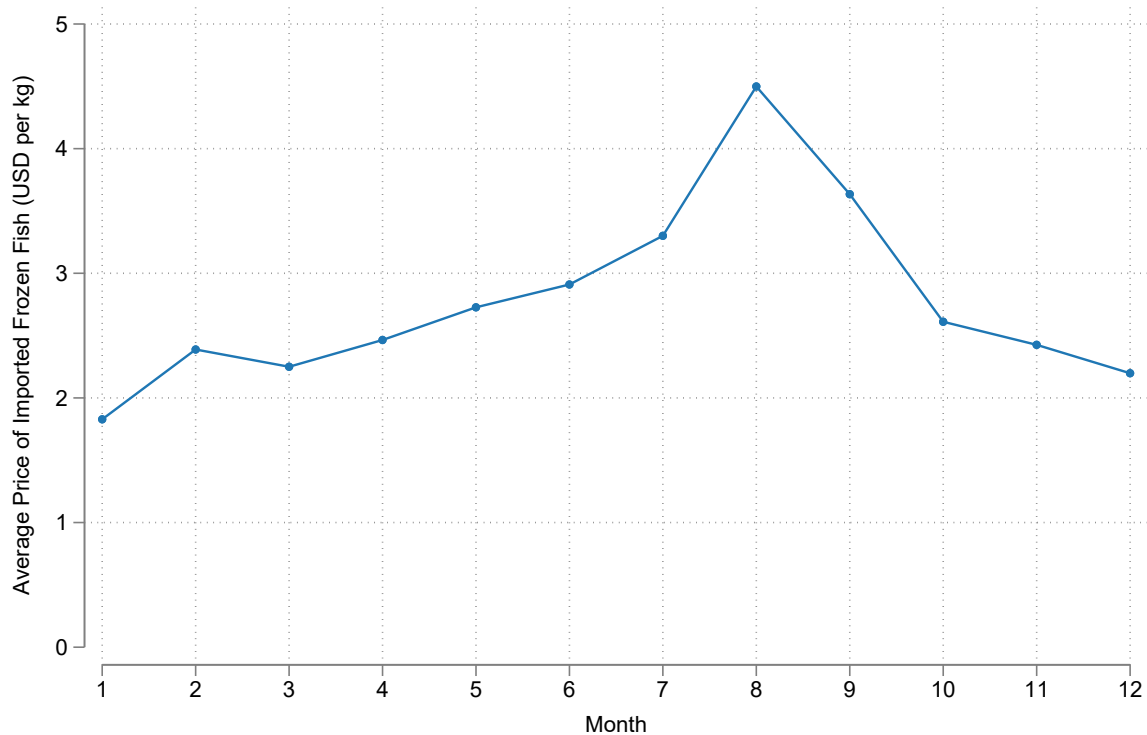
Notes: This figure presents regression discontinuity plots testing for discontinuities in oceanographic conditions around the start and end dates of China's fishing bans from 2012-2017. The top panels show  $\log$  chlorophyll-a concentration ( $\text{mg/m}^3$ ), and bottom panels show sea surface temperature ( $^{\circ}\text{C}$ ), both derived from NASA Ocean Color VIIRS satellite data at daily frequency. Left panels examine discontinuities when bans begin ("Ban ON"); right panels when bans end ("Ban OFF"). Data points represent daily zone-level averages aggregated from the original  $9 \text{ km} \times 9 \text{ km}$  resolution. The x-axis shows days relative to ban transitions, with day 0 marking the start/end of bans. Dashed lines show linear fits on each side of the cutoff. Nonparametric RD estimates and standard errors are reported for each discontinuity test.

Figure A.3: Placebo RDiT due to Shifting Start and End Dates of Fishing Ban



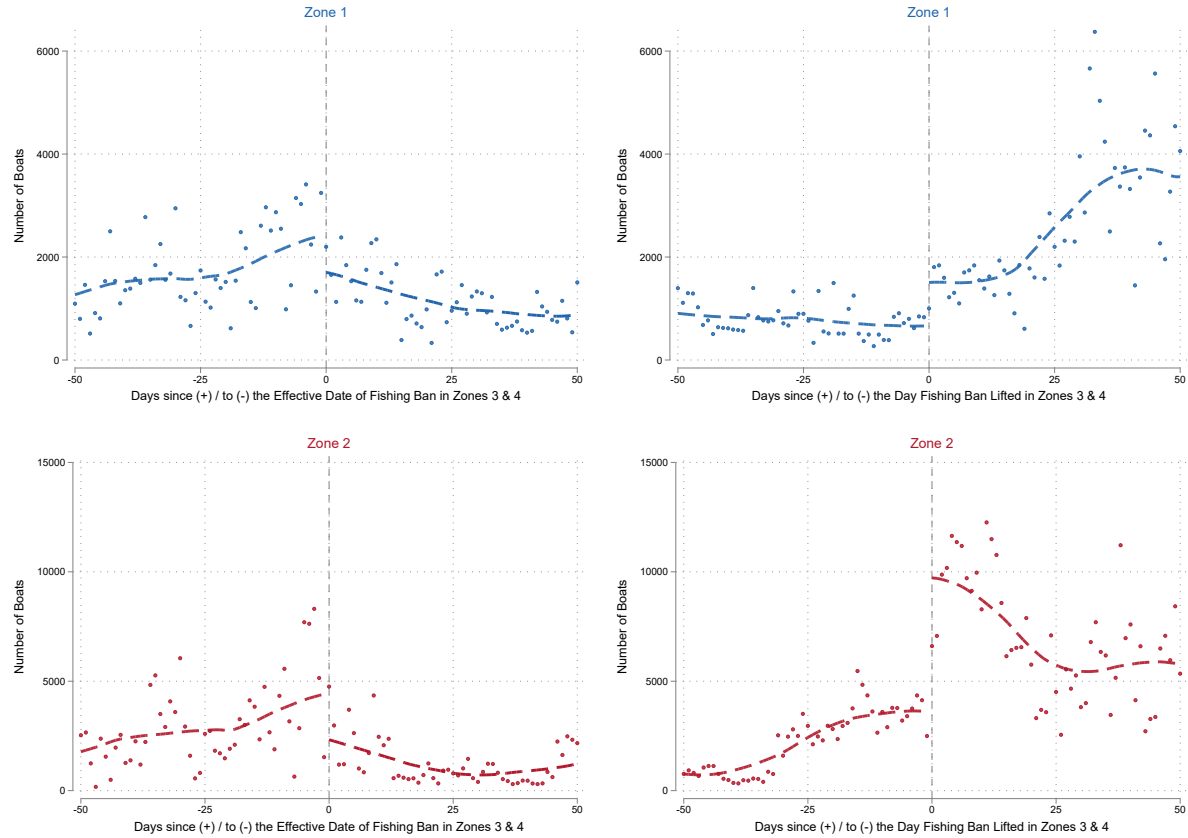
Notes: This figure presents placebo tests exploiting policy changes in China's seasonal fishing ban timing. The left panel examines the standardization of ban start dates to May 1st in 2017 (previously June 1st for Zones 1-2 and May 16th for Zones 3-4). The right panel examines the extension of ban end dates to August 16th in 2017 for Zones 3-4 (previously August 1st). Orange diamonds show daily boat detections in 2017-2018 when new dates applied; blue hollow circles show 2012-2016 when old dates applied. Day 0 marks May 1st in the left panel and August 16th in the right panel. The x-axis spans 20 days before and after these dates. Values represent average daily boat detections within each policy regime. Sample covers four regulatory zones where seasonal fishing bans are implemented. Running the same specifications as in Table 3 with the placebo dates yields no statistically significant estimates for the Fishing Ban indicator.

Figure A.4: Average Import Price of Frozen Fish into China



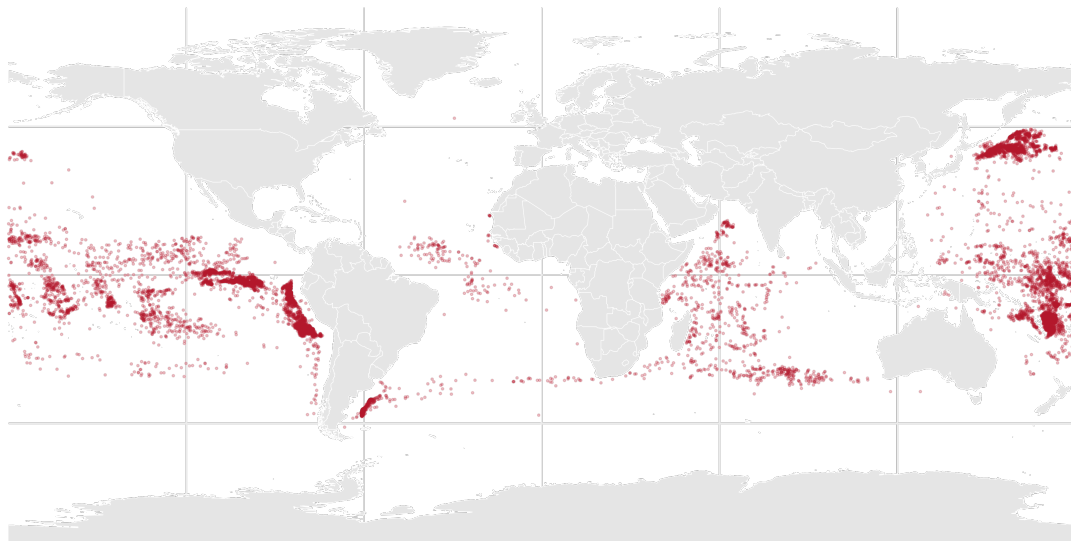
Notes: The figure shows the monthly average import price of frozen fish into China. The trade statistics are sourced from the United Nations Comtrade platform. China does not report import statistics to Comtrade at a monthly frequency. Instead, I accessed data via Comtrade's public API, using export values and volumes (weight) reported by the top 20 seafood exporters to China, based on annual trade data. The sample period spans from 2010 to 2017. Using data from these top 20 exporters, I calculated the average monthly import price of seafood in USD per kg. The top five seafood exporters to China during this period were Russia, the U.S., Canada, Norway, and New Zealand.

Figure A.5: Spillover from Zones 3 & 4 to Zones 1 & 2



Notes: The RD plots above apply the start and ending dates in Zones 3 & 4 to Zones 1 & 2. The subplots on the left hand side center on the starting of fishing bans in Zones 3 & 4; the subplots on the right hand side center on the lifting of fishing bans in Zones 3 & 4. Rows 1 to 2 represents Zones 1 to 2 respectively. Each dot represents the number of boat detections across the respective zone  $\tau$  nights since (+) or before (-) the fishing bans became effective (left subplots) or were lifted (right subplots) in Zones 3 & 4. Night 0 is the first night after the fishing bans were lifted in Zones 3 & 4 and the horizontal axis represents  $\tau$ . The vertical axis represents the nightly number of boat detections in Zone 1 or 2 aggregated over years from 2012 to 2017.

Figure A.6: Location of AIS Disabling Events of Chinese-flagged Vessels



Notes: This figure maps the locations of Automatic Identification System (AIS) disabling events for Chinese-flagged vessels from 2017–2020, based on data from Global Fishing Watch analyzed by [Welch et al. \(2022\)](#). Red dots indicate locations where vessels are suspected to have intentionally disabled their AIS transmissions. The full dataset includes over 55,000 suspected disabling events occurring more than 50 nautical miles from shore, identified using a rule-based machine learning classification model applied to 3.7 billion AIS messages. AIS disabling events by Chinese vessels appear concentrated in international waters, particularly near the Japanese and Peruvian EEZs, with notably fewer events occurring within or near China's own EEZ. This pattern suggests that AIS disabling behavior by Chinese vessels may be driven more by fishing opportunities in distant waters than by attempts to evade domestic regulations.

Table A.1: Fishing Ban and the Number of Boats Detected: Nonparametric RDiT Estimates

	Ban ON		Ban OFF	
	(1) # Boats	(2) log(# Boats)	(3) # Boats	(4) log(# Boats)
Aggregate (All Four Zones)				
Ban ON/OFF Switch	-8223.981*** (1091.375)	-1.291*** (0.133)	10701.150*** (2772.387)	0.623*** (0.157)
Obs.	151	151	151	151
Zone 1				
Ban ON/OFF Switch	-1277.873*** (350.677)	-0.959*** (0.292)	866.865 (653.745)	0.171 (0.224)
Obs.	151	151	151	151
Zone 2				
Ban ON/OFF Switch	-2089.284*** (606.819)	-1.901*** (0.263)	4739.264*** (1276.003)	0.875*** (0.239)
Obs.	151	151	151	151
Zone 3				
Ban ON/OFF Switch	-590.585*** (123.537)	-2.674*** (0.407)	910.553 (576.746)	0.465 (0.326)
Obs.	151	151	151	151
Zone 4				
Ban ON/OFF Switch	-4258.144*** (718.816)	-1.171*** (0.147)	3317.123*** (977.563)	0.316 (0.193)
Obs.	151	151	151	151

Notes: This table reports the nonparametric estimates of fishing bans on the number of boat detections in Columns (1) and (3), and on the log number of boat detections in Columns (2) and (4). Columns (1) and (2) report LATEs of the start of fishing bans. Columns (3) and (4) report LATEs of the lifting of fishing bans. Panels 2 to 5 from the top represent estimates for Zones 1 to 4 respectively. Each regulatory zone has one fishing ban each year. Over the sample period from 2012 to 2017, the 4 zones collectively have 24 fishing bans with varying duration. Daily boat detections with the same temporal distance to the fishing ban start/end are aggregated across sample years. Panel 1 also aggregates boat detections across regulatory Zones 1 to 4. The running variable is time measured in days relative to the fishing ban ON/OFF switching date. In Columns (1) and (2), the running variable is anchored at 0 when the fishing ban first became effective. In Columns (3) and (4), the running variable is anchored at 0 when the fishing ban was lifted. Nonparametric RD estimates are estimated using the bias-corrected local linear estimators proposed by [Calonico et al. \(2014\)](#), and standard errors are reported in the parentheses.

\*  $p < 0.10$ ; \*\*  $p < 0.05$ ; \*\*\*  $p < 0.01$ .

Table A.2: Fishing Ban and the Number of Boats Detected: Nonparametric Donut Hole RD Estimates

	Ban ON		Ban OFF	
	(1) # Boats	(2) log(# Boats)	(3) # Boats	(4) log(# Boats)
Aggregate (All Four Zones)				
Ban ON/OFF Switch	-10257.565*** (786.315)	-1.468*** (0.180)	11702.510 (11708.074)	0.962 (0.805)
Obs.	144	144	144	144
Zone 1				
Ban ON/OFF Switch	-2010.104*** (524.291)	-1.412*** (0.345)	1963.127 (1324.406)	0.878* (0.526)
Obs.	144	144	144	144
Zone 2				
Ban ON/OFF Switch	-3273.804*** (1156.968)	-2.027*** (0.622)	-1303.461 (4952.989)	-0.110 (1.055)
Obs.	144	144	144	144
Zone 3				
Ban ON/OFF Switch	-721.968 (483.771)	-0.378 (0.816)	985.421 (1248.124)	1.079 (1.024)
Obs.	144	144	144	144
Zone 4				
Ban ON/OFF Switch	-4847.571*** (1664.152)	-1.595*** (0.367)	9705.210** (4929.775)	1.339** (0.600)
Obs.	144	144	144	144

Notes: This table reports the nonparametric Donut Hole estimates of fishing bans on the number of boat detections in Columns (1) and (3), and on the log number of boat detections in Columns (2) and (4). Columns (1) and (2) report the Local Average Treatment Effects (LATEs) of the start of fishing bans. Columns (3) and (4) report the LATEs of the lifting of fishing bans. Panels 2 to 5 from the top represent estimates for Zones 1 to 4 respectively. Daily boat detections with the same temporal distance to the fishing ban start/end are aggregated across sample years. Panel 1 also aggregates boat detections across regulatory Zones 1 to 4. Each regulatory zone has one fishing ban each year. Over the sample period from 2012 to 2017, the 4 zones collectively have 24 fishing bans with varying duration. The running variable is time measured in days relative to the fishing ban ON/OFF switching date. In Columns (1) and (2), the running variable is anchored at 0 when the fishing ban first became effective, while in Columns (3) and (4), the running variable is anchored at 0 when the fishing ban was lifted. A 7-day window centered around the first night after the ban on/off switching is dropped from the estimation. Nonparametric Regression Discontinuity (RD) estimates are estimated using the bias-corrected local linear estimators proposed by [Calonico et al. \(2014\)](#), and standard errors are reported in the parentheses.

\*  $p < 0.10$ ; \*\*  $p < 0.05$ ; \*\*\*  $p < 0.01$ .

Table A.3: Fishing Ban and the Number of Boats Detected in Neighboring EEZs: Non-parametric RD Estimates

	Ban ON		Ban OFF	
	(1) # Boats	(2) log(# Boats)	(3) # Boats	(4) log(# Boats)
Aggregate (Neighbors of All Four Zones)				
Ban ON/OFF Switch	-1791.638** (753.250)	-0.201* (0.112)	2501.351* (1292.850)	0.238* (0.127)
Obs.	151	151	151	151
Zone 1 Neighbors				
Ban ON/OFF Switch	-392.609*** (111.890)	-0.372*** (0.110)	280.158 (361.882)	0.059 (0.217)
Obs.	151	151	151	151
Zone 2 Neighbors				
Ban ON/OFF Switch	-553.975*** (189.224)	-0.532*** (0.152)	470.575 (696.185)	0.182 (0.258)
Obs.	151	151	151	151
Zone 3 Neighbors				
Ban ON/OFF Switch	-628.880*** (231.152)	-1.112*** (0.319)	336.345 (378.163)	0.093 (0.328)
Obs.	151	151	151	151
Zone 4 Neighbors				
Ban ON/OFF Switch	-54.245 (720.103)	-0.042 (0.151)	1919.781*** (557.453)	0.616*** (0.163)
Obs.	151	151	151	151

Notes: This table reports the nonparametric RD estimates of fishing bans in China on boat detections in neighboring EEZs. The dependent variable is the number of boat detections in Columns (1) and (3), and is the log number of boat detections in Columns (2) and (4). Columns (1) and (2) report the LATEs of the start of fishing bans. Columns (3) and (4) report the LATEs of the lifting of fishing bans. Panels 2 to 5 from the top represent estimates for neighboring EEZs areas outside of Zones 1 to 4 respectively. Each regulatory zone has one fishing ban each year. Over the sample period from 2012 to 2017, the 4 zones collectively have 24 fishing bans with varying duration. Daily boat detections with the same temporal distance to the fishing ban start/end are aggregated across sample years. Panel 1 also aggregates boat detections across areas outside of regulatory Zones 1 to 4. The running variable is time measured in days relative to the fishing ban ON/OFF switching date. In Columns (1) and (2), the running variable is anchored at 0 when the related fishing ban first became effective, while in Columns (3) and (4), the running variable is anchored at 0 when the related fishing ban was lifted. Nonparametric RD estimates are estimated using the bias-corrected local linear estimators proposed by [Calonico et al. \(2014\)](#), and standard errors are reported in the parentheses.

\*  $p < 0.10$ ; \*\*  $p < 0.05$ ; \*\*\*  $p < 0.01$ .